

Analysis of factorization in $(e,e'p)$ reactions: A survey of the relativistic plane wave impulse approximation

J.A. Caballero^{1,2}, T.W. Donnelly³, E. Moya de Guerra² and J.M. Udías⁴

¹*Departamento de Física Atómica, Molecular y Nuclear
Universidad de Sevilla, Apdo: 1065, Sevilla 41080, SPAIN*

²*Instituto de Estructura de la Materia, Consejo Superior de Investigaciones Científicas
Serrano 123, Madrid 28006, SPAIN*

³*Center for Theoretical Physics, Laboratory for Nuclear Science and Dept. of Physics
Massachusetts Institute of Technology, Cambridge, MA 02139-4307, USA*

⁴*Departamento de Física Atómica, Molecular y Nuclear
Universidad Complutense de Madrid, Avda. Complutense s/n, Madrid 28040, SPAIN*

Abstract

The issue of factorization within the context of coincidence quasi-elastic electron scattering is reviewed. Using a relativistic formalism for the entire reaction mechanism and restricting ourselves to the case of plane waves for the outgoing proton, we discuss the meaning of factorization in the cross section and the role of the small components of the bound nucleon wave function.

PACS number(s): 25.30.Fj, 24.10.Jv, 21.10.Jx

Keywords: Nuclear reactions; Exclusive quasielastic electron scattering; Fully relativistic analysis; Positive and negative energy projection components

1. Introduction

As is well known [1] in standard plane-wave impulse approximation (PWIA) the differential cross section for A(e, e'p)B reactions factorizes into an elementary cross section σ_{ep} , describing electron proton scattering, and a spectral function $S(E_m, p_m)$, describing the probability for finding a proton in the target nucleus with energy (E_m) and momentum (p_m) compatible with the kinematics of the process. The differential cross section in PWIA is thus written as

$$\frac{d^6\sigma}{d\varepsilon' d\Omega_e dE_p d\Omega_p} = \chi\sigma_{ep} S(E_m, p_m) \quad (1)$$

with χ a kinematical factor. It is this factorization property that makes A(e, e'p)B reactions so appealing for investigations of nuclear structure.

According to eq. (1) single-particle distributions can in principle be probed in great detail. In fact several orbitals have been mapped out in many nuclei over rather extended momentum ranges [2]–[4], in spite of the limitations of the PWIA approximation. These limitations are also well known. Final-state interactions and, more generally, distortion of both electron and nucleon wave functions due to electromagnetic and strong interactions with target and residual nuclei destroy the elegant simplicity of eq. (1).

Nevertheless this equation is still very useful and is the basis for interpretation of experimental data. The latter are usually compared to theory defining an effective spectral function

$$\tilde{S}(E_m, p_m) = (\chi\sigma_{ep})^{-1} \frac{d^6\sigma}{d\varepsilon' d\Omega_e dE_p d\Omega_p} \quad (2)$$

and an effective proton momentum distribution (or reduced cross section [2, 3])

$$\tilde{\rho}(p_m) = \int_{\Delta E_m} \tilde{S}(E_m, p_m) dE_m, \quad (3)$$

that in PWIA corresponds exactly to the density in momentum space of the single-particle orbital associated with a selected value of the missing energy E_m . In general \tilde{S} and $\tilde{\rho}$ depend not only on p_m and E_m but also on the remaining kinematical variables.

Comparisons of theories taking into account in various ways final-state interactions and/or Coulomb distortions are also made for this effective momentum distribution. When

final-state interactions and Coulomb distortions are fully taken into account, departures between experiment and theory can solely be attributed to limitations of the single-particle nuclear model and impulse approximation. Thus eqs. (1) to (3) form also a basis for the empirical study of nucleon-nucleon correlations in the target.

In recent years much work has been done along these lines on both experimental and theoretical fronts. Experimental exclusive ($e, e'p$) measurements have been made with high precision on quite extensive missing momentum regions [2]–[4]. The analyses of data based on standard distorted-wave impulse approximation (DWIA) have met two major difficulties. On the one hand the spectroscopic factors extracted from DWIA analyses of low p_m ($p_m \leq 300$ MeV) data are too small compared with theoretical predictions. As an example the extracted occupations of $3s_{1/2}$ and $2d_{5/2}$ orbits in ^{208}Pb are $S_\alpha \simeq 0.5$, while theories on short-range correlations [5] predict at most a 30 % reduction of mean field occupations for levels just below the Fermi level. On the other hand the high- p_m data ($300 \text{ MeV} \leq p_m < 600 \text{ MeV}$) on $\tilde{\rho}(p_m)$ for the same levels are much larger than the results of DWIA calculations that are compatible with those that fit the low- p_m data [4]. Although short-range correlations are expected to increase the high momentum components, their effect is negligible [6] at the small missing energies of the existing high- p_m data, and effects of long-range correlations have been invoked [4]. The above mentioned DWIA analyses are based on non-relativistic independent particle models and use phenomenological (real and imaginary) Woods-Saxon potentials with parameters fitted to individual nuclei and shells.

Alternatively, in recent years, the relativistic mean field approximation has been successfully used for the analyses of both low- and high- p_m data [7]–[10]. In the relativistic distorted-wave impulse approximation (RDWIA) bound and scattered nucleons are described by solutions of the Dirac equation with scalar and vector (S-V) potentials. In the work of refs. [8]–[10] the scattering nucleon wave functions were obtained solving the Dirac equation with the relativistic optical potentials of ref. [11] and the bound nucleon wave functions were obtained with the TIMORA code [12] based on Walecka's mean field approximation [13]. The parameters of the S-V potentials are obtained from global fits and, at variance with DWIA, in RDWIA there were no parameters fitted to the particular levels

other than the spectroscopic factors. In all the cases studied the extracted spectroscopic factors are larger than in DWIA and are valid for low- and high- p_m data [7]–[10]. For instance, for the above mentioned $3s_{1/2}$ and $2d_{3/2}$ shells in ^{208}Pb values of $S_\alpha \simeq 0.7$ have been obtained [7, 8], consistent with theoretical predictions, and a reasonable agreement between RDWIA calculations and experiment has been found in the high- p_m region [10].

A global comparison of the unscaled results shows that, compared to DWIA, the reduced cross sections obtained in RDWIA are smaller at low p_m and are larger in the high- p_m region, thus providing a consistent description of all available data with moderate values of the spectroscopic factors.

The reasons why RDWIA produce smaller cross sections in the low- p_m region were investigated in refs. [9, 14]. In ref. [9] the success of the relativistic analyses was traced back to the improved treatment of distortion effects in the electron and outgoing proton waves. In the high p_m region other factors can be important. In particular, the presence of higher momentum components in the relativistic bound nucleon wave function, and in the relativistic nucleon current operator can be expected to play a role in this region. In view of the success of RDWIA calculations it is worthwhile investigating more deeply the dependence of the results on the lower components of the bound nucleon wave function and on the choice of the current operator. This is the purpose of this paper where we restrict ourselves to the relativistic plane-wave impulse approximation (RPWIA).

The reasons why we consider here only the plane-wave limit are twofold. On one hand it is convenient to restrict the study to RPWIA to be able to disentangle effects of distortion from effects of high p_m components in the bound nucleon wave function and current operator. On the other hand it is interesting to study this approximation because an important difference between relativistic and non-relativistic approaches already appears in the plane-wave limit. Namely, the factorized expression in eq. (1) does not necessarily hold in RPWIA. As we shall see in detail, this difference comes from the fact that in the non-relativistic approximation the nuclear current is expanded on a basis of free (positive energy) Dirac spinors, while in the relativistic approximation the nuclear current is directly written in terms of the relativistic bound nucleon wave function that contains both positive and negative energy projections in the complete Dirac basis. Thus

the question of whether factorization (in the sense of eq. (1)) does or does not hold in RPWIA is intimately connected with the role of the negative energy projection of the bound nucleon wave function.

Although the physical meaning of contributions from negative energy projections can be (and indeed is) a matter of debate [15], and their presence may be questioned, we would like to stress that in this respect our aim here is to analyze the quantitative importance of those contributions rather than to take sides on a particular conceptual interpretation or criterion.

As we shall see the extent to which negative energy components are important depends on the choice of the current operator. Thus the present analyses is also useful in choosing a particular form of the current operator once one adheres to a given criterion. For instance if one would like to follow the point of view that negative energy projections should not contribute to physical observables one would choose a current operator that minimizes the role of such components.

The organization of the paper is as follows. In section 2 we discuss in detail the relationship between RPWIA and PWIA differential cross sections. A separation of the RPWIA cross section and response functions is made into positive and negative energy projections. In section 3 we discuss various choices of the nuclear current operator and their influence on the positive and negative energy projections of the single-nucleon responses and cross sections. In section 4 we analyze the role of the negative energy projections and the lack of factorization in the total nuclear responses and differential cross sections. The main conclusions are summarized in section 5.

2. Formal comparison of RPWIA to PWIA

2.1 Differential cross section in RPWIA

The general formalism for exclusive electron scattering reactions has been presented in detail in several previous papers. We refer in particular to refs. [1] and [8] for the nonrelativistic and relativistic treatments, respectively. Here we just summarize the kinematics

and focus on those aspects of the cross section that are of relevance to the points of discussion in this paper.

In the (e,e'p) process an electron with four momentum $K^\mu = (\varepsilon, \mathbf{k})$ is scattered through an angle θ_e to four momentum $K'^\mu = (\varepsilon', \mathbf{k}')$. We denote the hadronic variables by $P_A^\mu = (M_A, \mathbf{O})$, $P_B^\mu = (E_B, \mathbf{p}_B)$, $P_N^\mu = (E_N, \mathbf{p}_N)$ the four momenta of the target, residual nucleus and outgoing proton, respectively. The target rest mass is M_A , and $M = \sqrt{E_N^2 - \mathbf{p}_N^2}$, $M_B = \sqrt{E_B^2 - \mathbf{p}_B^2}$ are the outgoing proton and residual nucleus masses (the latter may include possible internal excitation). As usual in these processes electrons are treated in the extreme relativistic limit (ERL): $\varepsilon = k$, $\varepsilon' = k'$. The four momentum transfer is given by $Q^\mu = K^\mu - K'^\mu = (\omega, \mathbf{q})$. For the applications discussed in the next sections we consider ^{16}O and have selected three kinematic situations:

- I) $q = 500 \text{ MeV}/c$, $\omega = 131.56 \text{ MeV}$
- II) $q = 1 \text{ GeV}/c$, $\omega = 432.8 \text{ MeV}$
- III) $q = 1 \text{ GeV}/c$, $\omega = 300 \text{ MeV}$.

The value of ω in kinematics I and II corresponds to the quasielastic peak value (ω_{QE}) while in kinematics III, $\omega < \omega_{QE}$, the so-called y -scaling region. Denoting by \mathbf{p} the three momentum of the struck nucleon ($\mathbf{p} = \mathbf{p}_m$, the missing momentum, in the RPWIA, as discussed below), the range of variation of p -values has been chosen $0 \leq p \leq 500 \text{ MeV}/c$. From similar arguments to those presented in ref. [16] it can be shown that the variation of the momentum p_N is negligible, since one has that $M_B^2 \gg p^2$. In fact, for $A = 16$ this variation is of the order of $\sim 4\%$ (kinematics I) and $\sim 1.5\%$ (kinematics II, III) in the whole range of p -values considered.

In order to compare the content of the relativistic and non-relativistic treatments in plane-wave impulse approximation we focus, without lack of generality, on the differential cross section leading to a specific final state of the residual nucleus, corresponding to proton knock-out from a specific bound orbital b in the target nucleus. Following ref. [8], and taking unity spectroscopic factors and plane waves for incoming electron and for outgoing electron and proton, we write the differential cross section in RPWIA as

$$\frac{d^5\sigma}{d\Omega_e d\varepsilon' d\Omega_N} = \frac{2\alpha^2}{Q^4} \left(\frac{\varepsilon'}{\varepsilon} \right) \frac{p_N M M_B}{M_A f_{rec}} 2 \overline{\sum} |\mathcal{M}|^2, \quad (4)$$

where $\overline{\sum}$ denotes average over initial and sum over final polarizations. The transition amplitude is the contraction of the electron (j_e^μ) and nucleon (J_N^μ) currents

$$\mathcal{M} = j_\mu^e J_N^\mu \quad (5)$$

with

$$j_e^\mu = \bar{u}_{\sigma_f}^e(\mathbf{k}') \gamma^\mu u_{\sigma_i}^e(\mathbf{k}) \quad (6)$$

$$J_N^\mu = \bar{u}_{\sigma_N}(\mathbf{p}_N) \hat{J}_N^\mu \Psi_b^{m_b}(\mathbf{p}), \quad (7)$$

where \hat{J}_N^μ is the nucleon current operator to be discussed in section 3 and the momentum and energy of the bound nucleon satisfy, $\mathbf{p} = \mathbf{p}_N - \mathbf{q} = -\mathbf{p}_B$; $\epsilon_b = -M_A + M_B + M = \omega - T_N - T_B$. The term $\Psi_b^{m_b}(\mathbf{p})$ denotes the Fourier transform of the relativistic bound nucleon wave function

$$\Psi_b^{m_b}(\mathbf{p}) = \frac{1}{(2\pi)^{3/2}} \int d\mathbf{p} e^{-i\mathbf{p}\cdot\mathbf{r}} \Psi_b^{m_b}(\mathbf{r}) \quad (8)$$

with $\Psi_b^{m_b}(\mathbf{r})$ a solution of the Dirac equation with S-V potentials. For details see appendix A and refs. [12, 13].

2.2 Positive and negative energy projections of the bound nucleon wave function and nucleon current

It is known that only free solutions can be expanded in terms of free positive-energy Dirac spinors u alone. For an interacting (i.e., not free) relativistic wave function there is always a coupling to the free negative-energy Dirac spinors v . This implies that the free relation between upper (u) and lower (d) components

$$\frac{\boldsymbol{\sigma} \cdot \mathbf{p}}{E + M} \phi^u = \phi^d \quad (9)$$

does not hold in general for a bound relativistic wave function. As we shall see in detail, this is what differentiates RPWIA from PWIA. To analyze this point we insert in eq. (7)

the completeness relation [17]

$$\sum_s [u_\alpha(\mathbf{p}, s)\bar{u}_\beta(\mathbf{p}, s) - v_\alpha(\mathbf{p}, s)\bar{v}_\beta(\mathbf{p}, s)] = \delta_{\alpha\beta} \quad (10)$$

and write

$$J_N^\mu = \langle J_N^\mu \rangle_u - \langle J_N^\mu \rangle_v, \quad (11)$$

where the first term, indicated by the index u , comes from the positive-energy projector involving the Dirac spinors $u(\mathbf{p}, s)$ and the second term, indicated by the index v comes from the negative-energy projector involving the Dirac spinors $v(\mathbf{p}, s)$. These contributions are given by

$$\langle J_N^\mu \rangle_u \equiv \langle J^\mu \rangle_u = \sum_s \bar{u}(\mathbf{p}_N, s_N) \hat{J}^\mu u(\mathbf{p}, s) [\bar{u}(\mathbf{p}, s) \Psi_b^{m_b}(\mathbf{p})] \quad (12)$$

$$\langle J_N^\mu \rangle_v \equiv \langle J^\mu \rangle_v = \sum_s \bar{u}(\mathbf{p}_N, s_N) \hat{J}^\mu v(\mathbf{p}, s) [\bar{v}(\mathbf{p}, s) \Psi_b^{m_b}(\mathbf{p})]. \quad (13)$$

To simplify the notation, here and in what follows we suppress the index N on nucleon currents and current operators.

Using the explicit expression of the relativistic bound nucleon wave function in momentum space given in appendix A, the u and v contractions in equations (12) and (13) are found to be

$$[\bar{u}(\mathbf{p}, s) \Psi_b^{m_b}(\mathbf{p})] = (-i)^\ell \sqrt{\frac{\bar{E} + M}{2M}} \alpha_{\kappa_b}(p) \langle s | \Phi_{\kappa_b}^{m_b}(\hat{\mathbf{p}}) \rangle \quad (14)$$

$$[\bar{v}(\mathbf{p}, s) \Psi_b^{m_b}(\mathbf{p})] = (-i)^\ell \sqrt{\frac{\bar{E} + M}{2M}} \beta_{\kappa_b}(p) \langle s | \Phi_{-\kappa_b}^{m_b}(\hat{\mathbf{p}}) \rangle, \quad (15)$$

where $\langle s | \Phi_{\pm\kappa_b}^{m_b}(\hat{\mathbf{p}}) \rangle$ indicates spin projections of the bispinors $\Phi_{\pm\kappa_b}^{m_b}$ on a spin state $|\frac{1}{2}s\rangle$, and the radial functions in momentum space α_{κ_b} and β_{κ_b} are given by

$$\alpha_{\kappa_b}(p) = g_{\kappa_b}(p) - \frac{p}{\bar{E} + M} S_{\kappa_b} f_{\kappa_b}(p) \quad (16)$$

$$\beta_{\kappa_b}(p) = \frac{p}{\bar{E} + M} g_{\kappa_b}(p) - S_{\kappa_b} f_{\kappa_b}(p) \quad (17)$$

with g_{κ_b} and f_{κ_b} the Bessel transforms of the standard upper and lower radial functions of the bound nucleon wave function in coordinate space (see appendix A for details).

Obviously for a free nucleon $\beta_\kappa(p) = 0$. For a bound nucleon $\beta_{\kappa_b}(p) \neq 0$ in general, unless we impose the relation in eq. (9) which amounts to imposing $\beta_{\kappa_b}(p) = 0$.

2.3 Tensorial decomposition

In order to connect with the standard PWIA we perform the usual decomposition of the transition probability in eq. (4) into a leptonic and a hadronic tensor

$$2\overline{\sum}|\mathcal{M}|^2 = \eta_{\mu\nu}W^{\mu\nu} \ , \quad (18)$$

where $\eta_{\mu\nu}$ is the leptonic tensor

$$\eta_{\mu\nu} = \sum_{\sigma_i\sigma_f} j_\mu^e j_\nu^{e*} \quad (19)$$

whose explicit expression can be found for instance in refs. [1, 18], and $W^{\mu\nu}$ is the hadronic tensor

$$W^{\mu\nu} = \frac{2}{2j_b + 1} \sum_{s_N m_b} J^\mu J^{\nu*} \ . \quad (20)$$

We recall that in standard PWIA the hadronic tensor factorizes into a tensor for elastic scattering on a free proton $\mathcal{W}^{\mu\nu}$ and the momentum distribution of the (non-relativistic) bound orbital $N_b(p)$

$$(W^{\mu\nu})_{PWIA} = \mathcal{W}^{\mu\nu}(\mathbf{p}, \mathbf{q})N_b(p) \quad (21)$$

with

$$\mathcal{W}^{\mu\nu}(\mathbf{p}; \mathbf{q}) = \sum_{s, s_N} \left[\overline{u}(\mathbf{p}_N, s_N) \hat{J}^\mu u(\mathbf{p}, s) \right]^* \left[\overline{u}(\mathbf{p}_N, s_N) \hat{J}^\nu u(\mathbf{p}, s) \right] \quad (22)$$

and

$$N_b(p) = \frac{1}{2j_b + 1} \sum_{m_b} |\phi_b^{m_b}(\mathbf{p})|^2 \ , \quad (23)$$

where $\phi_b^{m_b}(\mathbf{p})$ is the (non-relativistic) wave function of the bound nucleon in momentum space (see for instance refs. [1, 16, 19]).

The connection between RPWIA and PWIA can be best seen by substitution of eqs. (11-15) into eq. (20). This leads to the following expression for the hadronic tensor

$$W^{\mu\nu} = W_P^{\mu\nu} + W_N^{\mu\nu} + W_C^{\mu\nu} \ , \quad (24)$$

where $W_P^{\mu\nu}$ ($W_N^{\mu\nu}$) is the contribution from positive (negative) energy projections only, while $W_C^{\mu\nu}$ is a crossed term containing products of both positive and negative energy projections. These components of the hadronic tensor are given explicitly as follows

$$W_P^{\mu\nu} = \frac{2}{2j_b + 1} \sum_{m_b} \sum_{s_N} \langle \hat{J}^\mu \rangle_u^* \langle \hat{J}^\nu \rangle_u \quad (25)$$

$$W_N^{\mu\nu} = \frac{2}{2j_b + 1} \sum_{m_b} \sum_{s_N} \langle \hat{J}^\mu \rangle_v^* \langle \hat{J}^\nu \rangle_v \quad (26)$$

$$W_C^{\mu\nu} = \frac{-2}{2j_b + 1} \sum_{m_b} \sum_{s_N} \left(\langle \hat{J}^\mu \rangle_u^* \langle \hat{J}^\nu \rangle_v + \langle \hat{J}^\mu \rangle_v^* \langle \hat{J}^\nu \rangle_u \right) . \quad (27)$$

Using the relations

$$\sum_{m_b} \langle s | \Phi_{\kappa_b}^{m_b} \rangle^* \langle s' | \Phi_{\kappa_b}^{m_b} \rangle = \delta_{ss'} \frac{2j_b + 1}{8\pi} \quad (28)$$

$$\sum_{m_b} \langle s | \Phi_{\kappa_b}^{m_b} \rangle^* \langle s' | \Phi_{-\kappa_b}^{m_b} \rangle = -\langle s' | \boldsymbol{\sigma} \cdot \mathbf{p} | s \rangle \frac{2j_b + 1}{8p\pi} \quad (29)$$

it is easy to carry out the sum over m_b in eqs. (25-27) to get (see appendix B)

$$W_P^{\mu\nu} = N_{uu}(p) \mathcal{W}^{\mu\nu} \quad (30)$$

$$W_N^{\mu\nu} = N_{vv}(p) \mathcal{Z}^{\mu\nu} \quad (31)$$

$$W_C^{\mu\nu} = N_{uv}(p) \mathcal{N}^{\mu\nu} , \quad (32)$$

where we use the fact that in our case $\alpha_{\kappa_b}(p)$ and $\beta_{\kappa_b}(p)$ are real to write

$$N_{uu}(p) = (\tilde{\alpha}_{\kappa_b}(p))^2 \quad (33)$$

$$N_{vv}(p) = (\tilde{\beta}_{\kappa_b}(p))^2 \quad (34)$$

$$N_{uv}(p) = -2\tilde{\alpha}_{\kappa_b}(p)\tilde{\beta}_{\kappa_b}(p) \quad (35)$$

with

$$\tilde{\alpha}_{\kappa_b}(p) = \sqrt{\frac{E + M}{8\pi M}} \alpha_{\kappa_b}(p) \quad (36)$$

$$\tilde{\beta}_{\kappa_b}(p) = \sqrt{\frac{E + M}{8\pi M}} \beta_{\kappa_b}(p) \quad (37)$$

and the single-nucleon tensors $\mathcal{W}^{\mu\nu}$, $\mathcal{Z}^{\mu\nu}$, $\mathcal{N}^{\mu\nu}$ are given by

$$\mathcal{W}^{\mu\nu} = \text{Tr} \left[\left(\frac{\not{P} + M}{2M} \right) \bar{J}^\mu \left(\frac{\not{P}_N + M}{2M} \right) J^\nu \right] \quad (38)$$

$$\mathcal{Z}^{\mu\nu} = \text{Tr} \left[\left(\frac{\not{P} - M}{2M} \right) \bar{J}^\mu \left(\frac{\not{P}_N + M}{2M} \right) J^\nu \right] \quad (39)$$

$$\mathcal{N}^{\mu\nu} = \text{Tr} \left[\bar{J}^\mu \left(\frac{\not{P}_N + M}{2M} \right) J^\nu \gamma^0 \frac{\boldsymbol{\gamma} \cdot \mathbf{p}}{p} \frac{\not{P}}{2M} \right] , \quad (40)$$

where we use the notation $\bar{J}^\mu \equiv \gamma_0 J^{\mu+} \gamma_0$. Explicit expressions for these tensors for different current operators are given in appendix C.

As already mentioned $\mathcal{W}^{\mu\nu}$ is the usual single-nucleon tensor appearing in the standard PWIA for unpolarized scattering, while $\mathcal{Z}^{\mu\nu}$ and $\mathcal{N}^{\mu\nu}$ are new single-nucleon tensors that appear only when the bound nucleon wave functions contain a non-zero negative-energy projection. Using the identity

$$\boldsymbol{\gamma} \cdot \boldsymbol{p} = \boldsymbol{\sigma} \cdot \boldsymbol{p} \gamma_0 \gamma_5 \quad (41)$$

and following the arguments given in ref. [20] in the context of PWIA with polarized beam and target, it can be also shown that the single-nucleon tensor $\mathcal{N}^{\mu\nu}$ can be related to a diagonal tensor constructed from spinors quantized with respect to a spin axis pointing along a generic direction, $\mathcal{R}^{\mu\nu}(\theta_R, \phi_R)$, as

$$\mathcal{N}^{\mu\nu} \equiv \cos \theta \mathcal{R}^{\mu\nu}(0, 0) + \sin \theta \left(\cos \phi \mathcal{R}^{\mu\nu}\left(\frac{\pi}{2}, 0\right) + \sin \phi \mathcal{R}^{\mu\nu}\left(\frac{\pi}{2}, \frac{\pi}{2}\right) \right) \quad (42)$$

with θ, ϕ defining the direction of the bound nucleon momentum \boldsymbol{p} and

$$\mathcal{R}^{\mu\nu}(\theta_R, \phi_R) = \frac{1}{4M} \text{Tr} \left[\not{s}_L \bar{J}^\mu (\not{P}_N + M) J^\nu \right] \quad (43)$$

which is linear in the bound nucleon spin four-vector S_L^μ . The angles θ_R, ϕ_R define the direction of the spin \boldsymbol{s}_L in the frame in which the bound nucleon is at rest. The explicit expression of $\mathcal{R}^{\mu\nu}$ can be found in appendix C. Obviously this is not the only possible way to compute eq. (40) —we have used eqs. (42, 43) because explicit expressions for the $\mathcal{R}^{\mu\nu}$'s with the current operators that we consider here were already available.

2.4 Comparison of RPWIA and PWIA

In PWIA one defines a free electron proton cross section σ^{ep}

$$\sigma^{ep} = \frac{2\alpha^2 \varepsilon'}{Q^4} \frac{\eta_{\mu\nu}}{\varepsilon} \mathcal{W}^{\mu\nu} \quad (44)$$

to write the differential cross section as

$$\left(\frac{d^5 \sigma}{d\Omega_e d\varepsilon' d\Omega_N} \right)_{PWIA} = \frac{p_N M M_B}{M_A f_{rec}} \sigma^{ep} N_b(p) \quad (45)$$

with $N_b(p)$ the momentum distribution of the non-relativistic bound orbital (eq. (23)) normalized to 1 ($\int d\mathbf{p}N_b(p) = 1$).

In analogy, in RPWIA we may define single-nucleon cross sections σ_{uu}^{ep} , σ_{vv}^{ep} and σ_{uv}^{ep} corresponding to the single-nucleon tensors $\mathcal{W}^{\mu\nu}$, $\mathcal{Z}^{\mu\nu}$ and $\mathcal{N}^{\mu\nu}$ appearing in the $W_P^{\mu\nu}$, $W_N^{\mu\nu}$ and $W_C^{\mu\nu}$ hadronic tensors:

$$\sigma_{uu}^{ep} = \frac{2\alpha^2}{Q^4} \frac{\varepsilon'}{\varepsilon} \eta_{\mu\nu} \mathcal{W}^{\mu\nu} = \sigma^{ep} \quad (46)$$

$$\sigma_{vv}^{ep} = \frac{2\alpha^2}{Q^4} \frac{\varepsilon'}{\varepsilon} \eta_{\mu\nu} \mathcal{Z}^{\mu\nu} \quad (47)$$

$$\sigma_{uv}^{ep} = \frac{2\alpha^2}{Q^4} \frac{\varepsilon'}{\varepsilon} \eta_{\mu\nu} \mathcal{N}^{\mu\nu} . \quad (48)$$

Using the above definitions together with eqs. (18), (24) and (30)–(32) we can write the differential cross section in RPWIA (see eq. (4)) as

$$\frac{d^5\sigma}{d\Omega_e d\varepsilon' d\Omega_N} = \frac{p_N M M_B}{M_A f_{rec}} [\sigma_{uu}^{ep} N_{uu}(p) + \sigma_{vv}^{ep} N_{vv}(p) + \sigma_{uv}^{ep} N_{uv}(p)] , \quad (49)$$

where σ_{uu}^{ep} is the free electron-proton cross section appearing in eqs. (1) and (45) obtained from positive-energy projections, while σ_{vv}^{ep} and σ_{uv}^{ep} are new components that are solely due to the negative-energy projections and that may only appear in scattering from a bound nucleon. Thus, in RPWIA the differential cross section depends on both positive and negative energy projections of the relativistic bound nucleon wave function. Equation (49) is self-explanatory: it shows that one can perform a decomposition into a part proportional to the square of the positive-energy projection, N_{uu} , with proportionality factor σ_{uu}^{ep} . This proportionality factor involves only free u -Dirac spinors and it is identical to the standard σ^{ep} that appears in the non-relativistic treatment (see eq. (1)). The rest of the cross section is proportional (quadratically and linearly) to the negative-energy projection (N_{vv} or N_{uv}) and the proportionality factor involves (quadratically or linearly) free v -Dirac spinors.

From eq. (49) it is also a simple matter to go back to the *non-relativistic limit* by imposing condition (9) on the bound nucleon wave function. Indeed if we impose

$$\phi^d = \phi_{(0)}^d = \frac{\boldsymbol{\sigma} \cdot \mathbf{p}}{E + M} \phi^u \quad (50)$$

we get

$$\tilde{\alpha}_\kappa = \tilde{\alpha}_\kappa^{(0)} = \sqrt{\frac{2M}{E+M}} \frac{g_\kappa}{\sqrt{4\pi}} \quad (51)$$

$$\tilde{\beta}_\kappa = \tilde{\beta}_\kappa^{(0)} = 0 \quad (52)$$

and therefore all the terms containing negative-energy projections in eq. (49) become zero

$$N_{vv}^{(0)} = 0 \quad (53)$$

$$N_{uv}^{(0)} = 0 , \quad (54)$$

while the term depending only on positive-energy projections becomes

$$N_{uu}(p) = N_{uu}^{(0)}(p) = \frac{2M}{E+M} \frac{g_\kappa^2(p)}{4\pi} . \quad (55)$$

Thus, we recover eq. (49) with the non-relativistic momentum distribution $N_b(p)$ replaced by $N_{uu}^{(0)}(p)$ in eq. (55). Actually to go to the non-relativistic limit we should neglect terms of the order $(1 - \frac{E}{M})$ and therefore we write

$$N_{uu}^{n.r.}(p) = \frac{g_\kappa^2(p)}{4\pi} K , \quad (56)$$

where K is a normalization factor taking into account that $g_\kappa(p)$ is not normalized to 1 while $N_{uu}^{n.r.}(p)$ should be normalized to 1. Hence

$$K^{-2} = \int p^2 dp g_\kappa^2(p) . \quad (57)$$

We note that $K \geq 1$ because of the normalization condition of the relativistic bound nucleon wave function (see appendix A). Therefore in the non-relativistic limit the momentum distribution $N_{uu}^{n.r.}(p) \geq g_\kappa^2(p)/4\pi$. Actually since $f_\kappa^2(p)$ is small and does not contribute by more than a 3% to the normalization (for the case considered here $K = 1.025$) one has that $N_{uu}^{n.r.}(p) \approx N_{uu}^{(0)}(p)$ in the whole momentum range considered.

In Figure 1 we show the functions N_{uu} , N_{uv} and N_{vv} (in fm³) corresponding to the shell $1p_{1/2}$ in ¹⁶O. The bound state wave function for the proton has been computed within the framework of the Walecka relativistic model. The mean field in the Dirac equation is determined through a Hartree procedure from a phenomenological relativistic Lagrangian with scalar and vector (S-V) terms. We use the parameters of ref. [23], and the TIMORA

code [12] to get the radial functions g_{κ_b} , f_{κ_b} in coordinate space and then transform to momentum space according to the equations in appendix A.

In the left panel of fig. 1 we show the results for the three projection components of the momentum distribution $N_{uu}(p)$ (solid), $N_{uv}(p)$ (dotted) and $N_{vv}(p)$ (dashed) as given by eqs. (33–35). Note that the components N_{uu} and N_{vv} are positive whereas N_{uv} can be positive or negative depending on the p -value. This is specified by the signs (+)/(-). The component $N_{uu}(p)$ clearly dominates in the region $p \leq 300$ MeV/c. In fact, in the maximum ($p \sim 100$ MeV) it is one order of magnitude larger than the N_{uv} component and more than two orders of magnitude larger than the N_{vv} component. This suggests that in this region one can expect negligible contributions from the components $N_{uv}(p)$ and $N_{vv}(p)$. Therefore, for low p -values, one may expect that projecting the bound nucleon wave function over positive energy states gives basically the same result as a fully relativistic calculation. This assesment of course needs some care because in order to get final results one also needs to evaluate the single-nucleon components σ_{uu}^{ep} , σ_{uv}^{ep} and σ_{vv}^{ep} .

In the region of high missing momentum, $p > 300$ MeV/c, the situation is clearly different. In this p -region the values of the components $N_{uv}(p)$ and $N_{vv}(p)$ are similar to or even larger than that of $N_{uu}(p)$. Therefore, for $p > 300$ MeV/c one may expect that the effects of the dynamical enhancement of the lower components in the bound relativistic wave function will be observable.

It is also interesting to compare the positive-energy projection of the full relativistic bound wave function with the non-relativistic limits defined in eqs. (55,56). In the right panel of fig. 1 we compare the positive-energy projection $N_{uu}(p)$ (solid) with $N_{uu}^{(0)}(p)$ (eq. 55) (dotted line) and with $N_{uu}^{n.r.}(p)$ (eq. 56) (dashed line). Note that the difference between $N_{uu}^{(0)}(p)$ and $N_{uu}^{n.r.}(p)$ is negligible for all p -values. Moreover, the difference between these two functions and the component $N_{uu}(p)$ is only visible for $p \geq 400$ MeV/c. Since up to $p \simeq 400$ MeV there are no important differences between N_{uu} and $N_{uu}^{n.r.}$, we shall speak roughly of positive-energy projected and non-relativistic limits when discussing total nuclear responses and differential cross sections in section 4.

2.5 Longitudinal-Transverse separation

To finish with this section we note that one may also use the decomposition of currents into longitudinal and transverse components and then write the different projections of the σ 's as follows

$$\sigma_{uu}^{ep} = \sigma_{MOTT} \left(\sum_K v_K \mathcal{R}_{uu}^K \right) \quad (58)$$

$$\sigma_{vv}^{ep} = \sigma_{MOTT} \left(\sum_K v_K \mathcal{R}_{vv}^K \right) \quad (59)$$

$$\sigma_{uv}^{ep} = \sigma_{MOTT} \left(\sum_K v_K \mathcal{R}_{uv}^K \right) \quad (60)$$

with $K = L, T, TL, TT$ the longitudinal, transverse, TL interference and extra transverse contributions of the hadronic tensor for free nucleons. The single-nucleon responses \mathcal{R}_{uu}^K , \mathcal{R}_{vv}^K and \mathcal{R}_{uv}^K are given by taking the appropriate components of the single-nucleon tensors $\mathcal{W}^{\mu\nu}$, $\mathcal{Z}^{\mu\nu}$ and $\mathcal{N}^{\mu\nu}$, as is done for the R_{uu}^K in PWIA. It should be pointed out that contrary to the situation that occurs for on-shell nucleons, different results may be obtained depending on the choice of the current operator. In particular they depend on whether current conservation is or not imposed to eliminate one of the components, and on which of the 0- or 3- components is eliminated. This subject was discussed in detail in refs. [20, 21, 22] for the case of the \mathcal{R}_{uu}^K responses with and without polarizations and will be discussed in the next section for the \mathcal{R}_{uv}^K and \mathcal{R}_{vv}^K as well. Obviously, the hadronic response functions can be also written in RPWIA in the form

$$R^K = R_P^K + R_N^K + R_C^K \quad (61)$$

with each component given by

$$R_P^K = \mathcal{R}_{uu}^K N_{uu}(p) \quad (62)$$

$$R_N^K = \mathcal{R}_{vv}^K N_{vv}(p) \quad (63)$$

$$R_C^K = \mathcal{R}_{uv}^K N_{uv}(p) . \quad (64)$$

In standard PWIA only the responses \mathcal{R}_{uu}^K which are due solely to the positive-energy components occur. In this case, by dividing the experimental 5-differential cross section by

σ_{uu}^{ep} and the kinematical factors, one could measure directly the momentum distribution $N_{uu}(p)$. However, in the more general case of RPWIA, as we see in eqs. (49,61), this is not possible in general, as we have additional contributions from the negative-energy components that, *a priori*, cannot be isolated by experimental procedures. One could, however, study under what circumstances the results of eqs. (49,61) are dominated by some of the uu , vv or uv contributions. We present in detail this study in section 4 where results for the various observables of the scattering reaction are shown.

Analogously to the analysis within the standard PWIA [20, 21, 22], the evaluation of the three projection components of the various single-nucleon quantities depends on what single-nucleon current operator is chosen, on whether current conservation is fulfilled or imposed, and in the latter case on how it is imposed. This study is presented in detail in section 3, where different prescriptions involving single-nucleon current operators and the continuity equation are considered. Here we simply mention that there exist some kinematics for which the uu , vv or uv contributions to the single-nucleon cross section and single-nucleon response functions are comparable, and therefore a fully relativistic analysis can give very different results from the standard PWIA.

3. Current operators and single-nucleon responses

3.1 Choices of the current operator for bound nucleons

As discussed in several works [1, 20, 21, 22] the choice of the current operator $\hat{J}_N^\mu = \hat{J}^\mu$ is to some extent arbitrary. We discuss here the most popular choices denoted as CC1 and CC2 in ref. [21].

The current operator CC1

$$\hat{J}_{CC1}^\mu = (F_1 + F_2)\gamma^\mu - \frac{F_2}{2M} (\bar{P} + P_N)^\mu \quad (65)$$

with $\bar{P}^\mu = (\bar{E}, \mathbf{p})$ ($\bar{E} = \sqrt{\mathbf{p}^2 + M^2}$ and $\mathbf{p} = \mathbf{p}_N - \mathbf{q}$) is obtained from the current operator CC2

$$\hat{J}_{CC2}^\mu = F_1\gamma^\mu + i\frac{F_2}{2M}\sigma^{\mu\nu}Q_\nu \quad (66)$$

replacing Q_ν by $(P_N - \bar{P})_\nu$ and using the Gordon decomposition for the free nucleon case, i.e., assuming that initial and final nucleons in eq. (7) satisfy the free Dirac equation $(\not{P} - M)\Psi = 0$. For free nucleons eqs. (65) and (66) are totally equivalent and, since the current is conserved, the time component can be eliminated by writing it in terms of the third component or vice versa. In the case discussed here the final nucleon in eq. (7) satisfies the free Dirac equation, but the initial bound nucleon does not, and therefore the nucleon current and the nuclear responses are different when using CC1 or CC2 operators. Moreover the current is not conserved and, once the current operator (CC1 or CC2) has been chosen, one may choose to impose current conservation by eliminating the third component (CC1⁽⁰⁾ or CC2⁽⁰⁾), or the time component (CC1⁽³⁾ or CC2⁽³⁾). One may also choose not to impose current conservation (NCC1 or NCC2). In general each of these six different choices gives a different result and it is not clear how to define criteria that favour one choice over the others (see for instance [22]). In the absence of sharper criteria it is advisable to use as reference a current operator that guarantees current conservation for any initial and final nucleon wave function. For this purpose we choose the operator

$$\hat{J}_C^\mu = F_1 \gamma^\mu + i \frac{F_2}{2M} \sigma^{\mu\nu} Q_\nu - F_1 \frac{Q^\mu \not{Q}}{Q^2} \quad (67)$$

for $Q^2 < 0$, which is also equivalent to the CC1 and CC2 operators in the free nucleon case. Although we define the operator \hat{J}_C^μ only for the case of virtual photon ($Q^2 < 0$), we note that the last term in eq. (67) has no transverse component and therefore it does not contribute in the case of real photons anyway, where one could question its validity because of the divergence as $Q^2 \rightarrow 0$. This operator has several good features: a) with this operator the current in eq. (7) is conserved, and b) the amplitude \mathcal{M} in eq. (5) is invariant under the replacement of \hat{J}_C^μ by \hat{J}_{CC2}^μ because the electron current is conserved, which implies that the last term in eq. (67) does not contribute to the amplitude \mathcal{M} . A similar operator was introduced by Gross and Riska in ref. [24].

3.2 Comparison of different currents and single–nucleon responses

To understand better the results shown in the next sections it is helpful to split the amplitude in eq. (5) into its longitudinal (L) and transverse (T) components

$$\mathcal{M} = \mathcal{M}^L - \mathcal{M}^T \quad (68)$$

with

$$\mathcal{M}^L = j_e^0 \left(J^0 - \frac{w}{q} J^3 \right) \quad (69)$$

$$\mathcal{M}^T = \mathbf{j}_e^T \mathbf{J}^T = j_e^x J^x + j_e^y J^y \quad , \quad (70)$$

where we have taken the z -axis parallel to \mathbf{q} , and used the continuity equation for the electron current ($\omega j_e^0 = \mathbf{q} \cdot \mathbf{j}_e$). Now it is simple to check that the hadronic longitudinal current that we define for any current operator as

$$J^L = \left(J^0 - \frac{\omega}{q} J^3 \right) \quad (71)$$

is identical for the J_C^μ and J_{CC2}^μ choices. Indeed

$$J_C^L = \left(J_C^0 - \frac{w}{q} J_C^3 \right) = -\frac{Q^2}{q^2} J_C^0 = \left(J_{CC2}^0 - \frac{w}{q} J_{CC2}^3 \right) = J_{CC2}^L \quad . \quad (72)$$

On the other hand since the transverse components are equal,

$$\mathbf{J}_{CC2}^T = \mathbf{J}_C^T \quad , \quad (73)$$

both the longitudinal \mathcal{M}^L , and the transverse \mathcal{M}^T amplitudes (and hence each of the response functions) are invariant separately under the replacement of \hat{J}_C by \hat{J}_{CC2} . We emphasize that this is so provided that the complete expression for J_{CC2}^L in eq. (72) is used. We note however that if one starts from the CC2 operator and imposes current conservation (as done in the CC2⁽⁰⁾ and CC2⁽³⁾ versions), the longitudinal amplitude changes. In the CC2⁽⁰⁾ version, one replaces J_{CC2}^3 by $\frac{\omega}{q} J_{CC2}^0$ and therefore J_{CC2}^L is replaced by

$$J_{CC2}^L \rightarrow J_{CC2(0)}^L = \frac{-Q^2}{q^2} J_{CC2}^0 \quad . \quad (74)$$

Similarly in the CC2⁽³⁾ version one replaces J_{CC2}^0 by $\frac{q}{\omega} J_{CC2}^3$, or equivalently J_{CC2}^L is replaced by

$$J_{CC2}^L \rightarrow J_{CC2(3)}^L = \frac{q}{\omega} \left(\frac{-Q^2}{q^2} \right) J_{CC2}^3 . \quad (75)$$

In summary the NCC2 choice is equivalent to using the conserved current defined in eq. (67). To the contrary, with the CC2⁽⁰⁾ or CC2⁽³⁾ choices the \mathcal{M}^L amplitude becomes different and so do the response functions R^L and R^{TL} , while the transverse amplitude and response functions remain unchanged.

The effect of going from the conserved current to the CC2⁽⁰⁾ or CC2⁽³⁾ choices can be easily evaluated by considering the differences

$$\Delta_{CC2(0)}^L \equiv J_{CC2}^L - J_{CC2(0)}^L \quad (76)$$

and

$$\Delta_{CC2(3)}^L \equiv J_{CC2}^L - J_{CC2(3)}^L . \quad (77)$$

As expected they are both proportional to $\Psi_N \mathcal{Q} \Psi_i$, with different proportionality factors,

$$\Delta_{CC2(0)}^L = \frac{\omega^2}{q^2} F_1 \Psi_N \frac{\mathcal{Q}}{\omega} \Psi_i \quad (78)$$

$$\Delta_{CC2(3)}^L = F_1 \Psi_N \frac{\mathcal{Q}}{\omega} \Psi_i . \quad (79)$$

Similar relationships hold when the CC1⁽⁰⁾ and CC1⁽³⁾ currents are compared to NCC1, but in this case the differences $\Delta_{CC1(0)}^L$ and $\Delta_{CC1(3)}^L$ also contain a term proportional to $(1 - \bar{\omega}/\omega)$. Indeed when comparing $J_{CC1(0)}^L$ and $J_{CC1(3)}^L$ to J_{CC1}^L one gets

$$\Delta_{CC1(0)}^L \equiv J_{CC1}^L - J_{CC1(0)}^L = \bar{\Psi}_N \frac{\omega^2}{q^2} \left[(F_1 + F_2) \frac{\mathcal{Q}}{\omega} - \frac{F_2(E_N + \bar{E})}{2M} \left(1 - \frac{\bar{\omega}}{\omega} \right) \right] \Psi_i \quad (80)$$

$$\Delta_{CC1(3)}^L \equiv J_{CC1}^L - J_{CC1(3)}^L = \bar{\Psi}_N \left[(F_1 + F_2) \frac{\mathcal{Q}}{\omega} - \frac{F_2(E_N + \bar{E})}{2M} \left(1 - \frac{\bar{\omega}}{\omega} \right) \right] \Psi_i . \quad (81)$$

Obviously the transverse currents satisfy

$$\begin{aligned} J_{CC1(0)}^T &= J_{CC1(3)}^T = J_{CC1}^T \\ J_{CC2(0)}^T &= J_{CC2(3)}^T = J_{CC2}^T . \end{aligned}$$

Finally we compare NCC2 to NCC1. We note that \hat{J}_{CC2}^μ can be written without lack of generality as

$$\begin{aligned}\hat{J}_{CC1}^\mu - \hat{J}_{CC2}^\mu &= \frac{F_2}{2M} \left[\left\{ (M - \mathcal{P}_N)\gamma^\mu + \gamma^\mu(M - \overline{\mathcal{P}}) \right\} + (E + E_N - \overline{E} - \overline{E}_N)\delta_{\mu,0} \right] \\ &= \frac{F_2}{2M} \left[\left\{ (M - \mathcal{P}_N)\gamma^\mu + \gamma^\mu(M - \overline{\mathcal{P}}) \right\} - \delta_{\mu,i}(\omega - \overline{\omega})\gamma^0\gamma^i \right], i = 1, 2, 3 .\end{aligned}\tag{82}$$

From eq. (82) it is easy to see that all of the components are different for the NCC2 and NCC1 choices when Ψ_i is not a free u -spinor

$$J_{CC2}^\mu \neq J_{CC1}^\mu, \quad \mu = 0, 1, 2, 3\tag{83}$$

and

$$J_{CC2}^L \neq J_{CC1}^L\tag{84}$$

$$J_{CC2}^T \neq J_{CC1}^T .\tag{85}$$

We shall discuss these differences in more detail in the next subsection. However it is also interesting to compare the positive-energy projections of J_{CC2}^μ and J_{CC1}^μ (the u -parts defined in section 2). For the positive-energy projections one sees that

$$\langle J_{CC2}^0 \rangle_u = \langle J_{CC1}^0 \rangle_u\tag{86}$$

and

$$\langle J_{CC2}^i \rangle_{uu} = \langle J_{CC1}^i \rangle_{uu} + \frac{F_2}{2M}(\omega - \overline{\omega})\overline{u}_N\gamma^0\gamma^i u, \quad i = 1, 2, 3 .\tag{87}$$

Hence, when considering positive-energy projections one has that the time components are equal and the transverse and longitudinal components differ by an amount proportional to $\omega - \overline{\omega}$. This in turn implies that

$$\langle J_{CC2(0)}^L \rangle_u = \langle J_{CC1(0)}^L \rangle_u ,\tag{88}$$

while

$$\langle J_{CC2}^L \rangle_u - \langle J_{CC1}^L \rangle_u \propto (\omega - \overline{\omega})/2M\tag{89}$$

and

$$\langle J_{CC2}^T \rangle_u - \langle J_{CC1}^T \rangle_u = \langle J_{CC2(0)}^T \rangle_u - \langle J_{CC1(0)}^T \rangle_u = \langle J_{CC2(3)}^T \rangle_u - \langle J_{CC1(3)}^T \rangle_u \propto (\omega - \overline{\omega})/2M .\tag{90}$$

The above relationships are important in understanding how the different single-nucleon responses and the single-nucleon cross sections behave depending on the choice of the current operator and depending on whether we consider the positive-energy or negative-energy components. We show the behaviour of the various response functions for three different kinematical situations in figures 2–4. Figs. 2 and 3 are for kinematics I and II, respectively (see section 2). As seen in figs. 2a to 4a the longitudinal (L) and transverse-longitudinal (TL) responses tend to change for each of the current choices (NCC1, NCC2, CC1⁽⁰⁾, CC2⁽⁰⁾, CC1⁽³⁾ or CC2⁽³⁾), while the transverse responses (T and TT) only depend on whether the CC1 or the CC2 current operator is used (figs. 2b to 4b). This follows from the fact that the transverse current is independent of whether current conservation is imposed or not.

Let us first discuss the transverse responses whose behaviour is somewhat simpler to understand. We recall that NCC2 is equivalent to using the conserved current J_C^μ and therefore we use it as a reference. As seen in fig. 2b when CC2 (thick line) is replaced by CC1 (thin line) the positive-energy component of the transverse responses $\mathcal{R}_{uu}^{T,TT}$ changes little while the negative-energy components $\mathcal{R}_{uv}^{T,TT}$ and $\mathcal{R}_{vv}^{T,TT}$ differ by an order of magnitude or more. The reason for this is easily understood by looking at eq. (82). When considering the positive-energy component the first term in this equation becomes zero ($(\overline{P} - M)u = 0$) and the difference between the two curves for \mathcal{R}_{uu}^T is proportional to $(\omega - \overline{\omega})/2M$ (see eqs. (87), (90)); moreover in the interference response function \mathcal{R}_{uu}^{TT} the $(\omega - \overline{\omega})/2M$ dependence tends to cancel. On the contrary when one considers the negative-energy components $\mathcal{R}_{uv}^{T,TT}$ and $\mathcal{R}_{vv}^{T,TT}$ the first term in eq. (82) is maximum ($(\overline{P} + M)v = 2M$) and the difference between CC1 and CC2 is maximized. Although quantitative details depend on the kinematics, the same qualitative behaviour is seen in figs. 3b and 4b. It is also interesting to remark that with the CC2 choice the negative-energy components are of the same order as the positive-energy ones in the whole p -region considered, while with the CC1 current (because of $(M - \overline{P})$ terms) the uv and vv components may become much larger than the uu ones. Hence one can expect a stronger dependence on the negative-energy projections β_κ when using the CC1 operator.

These trends are also observed in the longitudinal and longitudinal-transverse re-

sponses (figs. 2a to 4a). The CC1 current gives similar responses as the CC2 current for the uu components, but for the uv and vv components, the CC1 current tends to give much larger results (for the absolute values). In addition, a very important role is played by the way in which current conservation is imposed (or not). If one chooses not to impose current conservation (NCC1 or NCC2) one observes the same qualitative behaviour as that just discussed for the transverse components. The choice of imposing current conservation by elimination of the third component (CC1⁽⁰⁾ and CC2⁽⁰⁾) also shows a behaviour similar to that discussed above and the results tend to be close to the NCC1, NCC2 responses. Particularly in this case CC1⁽⁰⁾ and CC2⁽⁰⁾ give identical results for the uu component (as is clear from eq. (88)). However the CC1⁽³⁾ and CC2⁽³⁾ choices cause large deviations in all of the components including the positive-energy components $\mathcal{R}_{uu}^{L,TL}$, particularly for kinematics II. This behaviour is mainly due to the $\Psi_i \not{Q} \Psi_f$ term in eqs.(79,81) that (as seen in figs. 2a to 4a) may cause a strong reduction of the $\mathcal{R}_{uu}^{L,TL}$ responses when one goes from NCC1 to CC1⁽³⁾ or from NCC2 to CC2⁽³⁾. This reduction is also present in the CC1⁽⁰⁾ and CC2⁽⁰⁾ choices, but in these cases it is largely attenuated by the ω^2/q^2 factor in eqs. (78,80) and therefore the latter choices give results much closer to the NCC2 result that we use as reference.

It is important to remark that the simple relations stated in eqs. (78–81) are also responsible for the large differences observed between results obtained with CC1⁽⁰⁾ and CC1⁽³⁾ choices (or with CC2⁽⁰⁾ and CC2⁽³⁾) in the context of PWIA (see refs. [20, 21, 22]). In these references the study was restricted to σ^{ep} (or its various polarization components), although the cause of the large differences was not as clearly identified as it is here. In particular, the following interesting relationship between TL responses follows:

$$\frac{\mathcal{R}_{CCi}^{TL} - \mathcal{R}_{CCi(0)}^{TL}}{\mathcal{R}_{CCi}^{TL} - \mathcal{R}_{CCi(3)}^{TL}} = \frac{\omega^2}{q^2} \ll 1, \quad i = 1, 2. \quad (91)$$

A more involved relationship can be established for the \mathcal{R}^L responses obtained with different choices.

The single-nucleon cross section components σ_{uu}^{ep} , σ_{uv}^{ep} and σ_{vv}^{ep} are also shown for completeness in figs. 5 and 6. The results shown correspond to a redefinition of the σ 's including the factor $M^2/\overline{E}E_N$ for easy comparison to previous work along similar lines,

i.e.,

$$\tilde{\sigma}_{uu}^{ep} = \frac{M^2}{\bar{E}E_N} \sigma_{uu}^{ep} = \sigma^{ep} \quad (92)$$

with σ^{ep} as defined by de Forest [21]. Similar definitions are used for $\tilde{\sigma}_{uv}^{ep}$ and $\tilde{\sigma}_{vv}^{ep}$ in terms of σ_{uv}^{ep} and σ_{vv}^{ep} , respectively.

Fig. 5 corresponds to kinematics I for $\theta_e = 30^\circ$ (top panel) and $\theta_e = 150^\circ$ (lower panel) and fig. 6 corresponds to kinematics II with $\theta_e = 12.5^\circ$ (the forward-angle limit of the Hall A spectrometers at CEBAF). For the positive-energy components (σ_{uu}^{ep}) the dependence on the different choices of the current operator is maximal for kinematics I and forward angle. For kinematics II that dependence remains small at any angle. The dependence of $\tilde{\sigma}_{uu}^{ep}$ (i.e., σ^{ep}) on the current operator has been discussed at length in refs. [20, 21, 22]. Much more notorious is the dependence of σ_{uv}^{ep} and σ_{vv}^{ep} on the various current choices. Obviously the behaviour of the single-nucleon cross sections at 30° in fig. 5 mainly reflects the behaviours of \mathcal{R}^L (and partly of \mathcal{R}^{TL}), while the behaviour of σ 's at $\theta_e = 150^\circ$ (bottom in fig. 5) mainly results from the interplay between \mathcal{R}^{TL} and \mathcal{R}^T responses. Compared to the wild variation of σ_{uv}^{ep} and σ_{vv}^{ep} , σ_{uu}^{ep} shows a rather mild dependence on the choice of current operator.

We would like to emphasize that the changes in σ_{uu}^{ep} are minor for NCC1, NCC2, CC1⁽⁰⁾ and CC2⁽⁰⁾ and are important for CC1⁽³⁾ and CC2⁽³⁾, particularly at small q (kinematics I). As one increases q ($q \geq 1$ GeV) the latter choices may not be that poorly behaved.

It is also important to remark here that the single-nucleon cross sections associated with the negative-energy projections (σ_{uv}^{ep} and σ_{vv}^{ep}) tend to be larger in absolute values when the CC1 current operator is used. Therefore one may expect a larger effect of the negative-energy projections in the total differential cross sections when using \hat{J}_{CC1}^μ , and therefore a larger deviation from the non-relativistic PWIA result.

3.3 The effect of S–V potentials

We now study in detail the problem of different current operator choices for nucleons satisfying the Dirac equation with S–V potentials

$$(\not{P} - M - V\gamma_0 + S)\Psi = 0 \quad . \quad (93)$$

In principle both initial and final nucleons could be considered as solutions of this equation with the same potential; however, in the present work to simplify the problem somewhat in discussing the situation where the final nucleon is at relatively high energies (and so roughly quasifree) here we concentrate on the case (RPWIA) in which the outgoing nucleon is a solution of the free Dirac equation. Thus for the final wave function we have

$$(\not{P} - M)\Psi_f = 0 \quad , \quad (94)$$

while for the initial

$$(\not{P} - M)\Psi_i = (V\gamma_0 - S)\Psi_i \quad . \quad (95)$$

To understand the effect of the S-V potentials in the initial state we first write the wave function in coordinate space

$$\Phi(x_\mu) = e^{-iEt}\Psi(\mathbf{x}) = e^{-iEt} \begin{pmatrix} \phi_u(\mathbf{x}) \\ \phi_d(\mathbf{x}) \end{pmatrix} \quad (96)$$

with

$$\phi_d(\mathbf{x}) = \frac{\boldsymbol{\sigma} \cdot \mathbf{p}\phi_u(\mathbf{x})}{\tilde{E}(\mathbf{x}) + \tilde{M}(\mathbf{x})} \quad , \quad (97)$$

where $\mathbf{p} = -i\nabla$ and

$$\begin{aligned} \tilde{E}(\mathbf{x}) &= E - V(x) = \tilde{E}(x) \\ \tilde{M}(\mathbf{x}) &= M - S(x) = \tilde{M}(x) \quad . \end{aligned} \quad (98)$$

For S and V constant (nuclear matter) the solutions are still plane waves satisfying

$$\tilde{E}_0 = \sqrt{\mathbf{k}^2 + \tilde{M}_0^2} \quad (k \leq k_F) \quad , \quad \tilde{E}_0 = E - V_0 \quad , \quad \tilde{M}_0 = M - S_0 \quad , \quad (99)$$

while for S and V x -dependent the solutions satisfy the standard equations

$$\begin{aligned} \nabla^2 \phi_u(\mathbf{x}) &= -(\tilde{E}^2 - \tilde{M}^2)\phi_u - i\eta'(x)\boldsymbol{\sigma} \cdot \mathbf{x}\phi_d \\ \nabla^2 \phi_d(\mathbf{x}) &= -(\tilde{E}^2 - \tilde{M}^2)\phi_d + i\eta(x)\boldsymbol{\sigma} \cdot \mathbf{x}\phi_u \end{aligned} \quad (100)$$

with

$$\begin{aligned} \eta' &= \frac{1}{x} \frac{d}{dx}(S + V) \\ \eta &= \frac{1}{x} \frac{d}{dx}(S - V) \quad . \end{aligned} \quad (101)$$

We are interested in working in momentum space and thus write (see also appendix A)

$$\phi_u(\mathbf{p}) = \frac{1}{(2\pi)^{3/2}} \int d\mathbf{x} e^{-i\mathbf{p}\cdot\mathbf{x}} \phi_u(\mathbf{x}) \quad (102)$$

$$\phi_d(\mathbf{p}) = \frac{1}{(2\pi)^{3/2}} \int d\mathbf{x} e^{-i\mathbf{p}\cdot\mathbf{x}} \phi_d(\mathbf{x}) = \frac{1}{(2\pi)^{3/2}} \int d\mathbf{x} e^{-i\mathbf{p}\cdot\mathbf{x}} \frac{(-i\boldsymbol{\sigma}\cdot\nabla\phi_u(\mathbf{x}))}{\tilde{E} + \tilde{M}}. \quad (103)$$

We now write (either in \mathbf{p} or \mathbf{r} -space)*

$$\Psi = \left[\begin{pmatrix} 1 \\ \frac{\boldsymbol{\sigma}\cdot\mathbf{p}}{\tilde{E}+M} \end{pmatrix} \phi_u + \delta\Psi \right] \quad (104)$$

with

$$\delta\Psi = \begin{pmatrix} 0 \\ \phi'_d \end{pmatrix} \quad (105)$$

and

$$\phi'_d = \phi_d - \frac{\boldsymbol{\sigma}\cdot\mathbf{p}}{\tilde{E} + M} \phi_u. \quad (106)$$

The first term in eq. (104) is proportional to the positive-energy projection of Ψ (it has zero negative-energy projection), while the second term is a correction proportional to the negative-energy projection of Ψ . We use this decomposition to analyze the dependence on the dynamical enhancement (ϕ'_d) of the bound nucleon wave function when different choices of the current operator are used.

We start as before from CC2 and CC1 and particularize to the present initial and final nucleon wave functions satisfying eqs. (95) and (94), respectively. Using eq. (82) together with eqs. (94) and (95) we find that

$$J_{CC2}^\mu - J_{CC1}^\mu = \frac{F_2}{2M} \bar{\Psi}_f \left[\gamma^\mu (V\gamma^0 - S) + (\omega - \bar{\omega})\delta_{\mu,0} \right] \Psi_i \quad (107)$$

with $\omega - \bar{\omega} = \bar{E} - E$, $\bar{E} = \sqrt{p^2 + M^2}$ and E the energy of the bound nucleon wave function ($E = E_N - \omega = M_A - M_B^*$, neglecting the recoil energy of the residual nucleus). Hence if

*In this section \mathbf{p} is used both for operator (when writing in \mathbf{r} -space) and as c-number (when writing in momentum space)

we write down explicitly the $\mu = 0, 1, 2, 3$ components we find that

$$J_{CC2}^0 - J_{CC1}^0 = \frac{F_2}{2M} \bar{\Psi}_f [V - S\gamma^0 + (\omega - \bar{\omega})] \Psi_i \quad (108)$$

$$J_{CC2}^3 - J_{CC1}^3 = \frac{F_2}{2M} \bar{\Psi}_f [\gamma^3(V\gamma^0 - S)] \Psi_i \quad (109)$$

$$\mathbf{J}_{CC2}^\perp - \mathbf{J}_{CC1}^\perp = \frac{F_2}{2M} \bar{\Psi}_f [\boldsymbol{\gamma}^\perp(V\gamma^0 - S)] \Psi_i . \quad (110)$$

For the longitudinal components that enter in NCC2 and NCC1 one gets:

$$\begin{aligned} J_{CC2}^L - J_{CC1}^L &= \frac{F_2}{2M} \bar{\Psi}_f \left[V - S\gamma^0 + (\omega - \bar{\omega}) - \frac{\omega}{q} \gamma^3(V\gamma^0 - S) \right] \Psi_i \\ &= \frac{F_2}{2M} \bar{\Psi}_f \left([V - S + \omega - \bar{\omega}] \phi_u + \frac{\omega}{q^2} \boldsymbol{\sigma} \cdot \mathbf{q} (V + S) \phi_d \right) \\ &\quad \left(\frac{\omega}{q^2} \boldsymbol{\sigma} \cdot \mathbf{q} (V - S) \phi_u + [V + S + \omega - \bar{\omega}] \phi_d \right) \end{aligned} \quad (111)$$

Hence there are in general three types of terms in the difference between the longitudinal CC2 and CC1 currents:

- One proportional to $\omega - \bar{\omega}$ that is present even after projection into the positive-energy sector. We recall that only in CC1⁽⁰⁾ and CC2⁽⁰⁾ choices the longitudinal currents are equal for the positive-energy projections (see eq. (89)).
- One proportional to the SMALL nuclear $(V - S)$ potential acting on the upper component ϕ_u .
- One proportional to the LARGE nuclear potential $(S + V)$ acting on the down component ϕ_d .

The latter contribution tends to enhance the role of the negative-energy components. In other words any dynamical enhancement ϕ'_d of the lower component of the bound nucleon wave function may appear unphysically augmented in the nuclear response due to lack of current conservation. Similar considerations apply to the difference between the transverse CC2 and CC1 currents,

$$J_{CC2}^x - J_{CC1}^x = \frac{F_2}{2M} \begin{pmatrix} -\sigma^x(V + S)\phi_d \\ \sigma^x(V - S)\phi_u \end{pmatrix} \quad (112)$$

4. Dependence of the response functions and reduced cross sections on the negative energy projections

In this section we present results of response functions and differential cross sections for $1p_{1/2}$ proton knock-out from ^{16}O . The aim here is to make a quantitative analysis of the relative importance of negative-energy projection contributions for various choices of the current operator.

The total hadronic response functions in RPWIA are shown in fig. 7. We have chosen kinematics I and the forms of current operators discussed in section 3. As already mentioned in that section the transverse responses (R^T and R^{TT}) depend only on whether the current operator CC1 or CC2 is chosen, while the R^L and R^{TL} responses depend also on the current conservation prescription. We recall that NCC2 is equivalent to using an exactly conserved current.

As expected the longitudinal response R^L is practically identical for NCC2, CC1⁽⁰⁾ and CC2⁽⁰⁾ (also for NCC1, not shown), while it is substantially different for CC2⁽³⁾. It is interesting to note that, unlike in PWIA, in RPWIA the longitudinal response R^L for CC1⁽³⁾ is closer to the CC1⁽⁰⁾ than to the CC2⁽³⁾ cases. The shift upwards of R^L in the CC1⁽³⁾ case is due to the negative-energy projection R_N^L because, as seen in fig. 2a, the \mathcal{R}_{vv}^L single-nucleon response is much larger than \mathcal{R}_{uu}^L , compensating for the smallness of the negative-energy projection of the wave function (N_{vv}) (see fig. 1). Clearly if we were to consider only positive-energy projections, similar results would be obtained with CC1⁽³⁾ and CC2⁽³⁾ (as is the case in PWIA) —the term \mathcal{R}_{vv}^L is roughly an order of magnitude larger with CC1⁽³⁾ than with CC2⁽³⁾ causing a larger longitudinal response for the relativistic bound nucleon. In the longitudinal response function R^L the contributions of the negative-energy projections are maximized for CC1⁽³⁾, are minimized for NCC2 and are also negligible for CC1⁽⁰⁾ and CC2⁽⁰⁾. This is illustrated in the top panel of fig. 8 where R_P^L , R_N^L and R_C^L are plotted separately for various current choices. Here we use P , N and C to denote positive, negative and cross terms, respectively. In the CC1⁽³⁾ case R_P^L is only 80% of the total R^L , while for the other choices R_P^L is more than 95% of the total (see also figs. 10, 11).

As seen in fig. 7 the R^{TL} response is the one where the effects of different prescriptions for the nucleon current are the largest. The maximum of this response can change by as much as a factor of 2 (or 3) when one goes from CC1⁽³⁾ to CC2⁽³⁾ and CC1⁽⁰⁾ (or to CC2⁽⁰⁾). Here one can see with the help of the lower panel of fig. 8 (see also figs. 10, 11) that the negative-energy projections of the bound nucleon play a very important role through the crossed term R_C^{TL} , while R_N^{TL} remains negligible. This follows from the fact that in the p region under study, \mathcal{R}_{uv}^{TL} is of the same order as \mathcal{R}_{vv}^{TL} and much larger than \mathcal{R}_{uu}^{TL} (see fig. 3a). As in the case of R^L also for R^{TL} the negative-energy contributions are minimal with the CC2⁽⁰⁾ choice and maximal with the CC1⁽³⁾ choice. With this latter choice the negative-energy contribution R_C^{TL} is dominant, contributing by $\sim 75\%$ to the total R^{TL} , with CC1⁽⁰⁾ and CC2⁽³⁾ choices R_C^{TL} and R_P^{TL} contributions are approximately equal and even with the CC2⁽⁰⁾ choice the R_C^{TL} cross term gives a sizable ($\sim 30\%$) contribution. Since for all the choices the positive-energy projections in the maximum are similar, the net R^{TL} responses in RPWIA vary strongly from one choice to the other. Since relativistic effects are so important in this response, even in the plane-wave limit discussed here, it is likely that experimental data may reveal such effects.

For the transverse responses R^T and R^{TT} the differences seen in fig. 7 between CC1 and CC2 results are solely due to the negative-energy projections (see also figs. 9,10,11). Again, these contributions ($R_C^{T,TT}$, $R_N^{T,TT}$) are maximal for the CC1 choice. However, in the case of R^T their total contribution at the maximum is less than 10% for CC1 and less than 3% for CC2. Relatively much larger are the contributions of the negative-energy projections to R^{TT} , although this response is very small compared to R^T and it is difficult to isolate R^{TT} from differential cross section measurements.

Focusing on the choices CC1⁽⁰⁾ and CC2⁽⁰⁾ that are closer to NCC2, in all cases we show in figs. 10 and 11, respectively, the total R^K responses and their P , N and C terms to better appreciate the relative importance of the negative-energy projections in each response function. Clearly for the large responses R^L and R^T the difference between the total relativistic responses and their positive-energy projection is negligible. This in turn implies that for these responses one cannot expect to see large effects in going from PWIA to RPWIA, since also $N_{uu} \approx N_{uu}^{n.r.}$. Hence the factorization limit of PWIA is practically

preserved by RPWIA in the R^L and R^T responses except when the $CC1^{(3)}$ prescription is used for the current. On the contrary, the small response R^{TT} and the longitudinal transverse response R^{TL} are very sensitive to contributions from the negative-energy components, because the contributions from positive-energy projections are relatively small. For these responses the factorization limit of PWIA is badly broken even when the more conservative $CC2^{(0)}$ choice is used (see fig. 11).

The breaking of this PWIA factorization limit in RPWIA has important consequences in the differential cross section. This is illustrated in figs. 12–14 for different kinematical situations. Fig. 12 is for kinematics I at two different electron scattering angles (left $\theta_e = 30^\circ$, right $\theta_e = 150^\circ$), while figs. 13,14 are for kinematics II and III at forward angle ($\theta_e = 12.5^\circ$). We compare the fully relativistic results given by the prescriptions $CC1^{(0)}$ (thin–solid), $CC2^{(0)}$ (thick–solid), $CC1^{(3)}$ (thin–dash) and $CC2^{(3)}$ (thick–dash) to the non-relativistic PWIA limit (dotted). The PWIA results in these figures have been calculated from eq. (45) with $N_b(p)$ as given by $N_{uu}^{n.r.}(p)$ in eq. (56) and with the $CC1^{(0)}$ choice. It is important to stress here that these PWIA results practically coincide with the positive-energy projection contribution of the total RPWIA differential cross section in eq. (49). Indeed the difference comes only from the difference between $N_{uu}(p)$ (eq. (33)) and $N_{uu}^{n.r.}(p)$ (eq. (56)), which is negligible, as seen in the right-hand panel of fig. 1. Hence the differences between the dotted and thin–solid ($CC1^{(0)}$) lines in figs. 12–14 are due to the contributions from the negative-energy projections. Differences with thick–solid ($CC2^{(0)}$), thick–dash ($CC2^{(3)}$), and thin–dash ($CC1^{(3)}$) are also partly due to the effect of the negative-energy contributions and partly due to the different current operator.

Clearly seen in these figures is the fact that there are two important effects of the negative-energy projections of the bound nucleon wave function: A) A modification of the strength of the peak at low p ($p < 300$ MeV), where data are used to determine spectroscopic factors (particularly important for kinematics I and for the prescriptions $CC1^{(3)}$ and $CC2^{(3)}$); B) A substantial modification of the shape of the differential cross section, particularly in the high p region. This latter effect is apparent in all of the different kinematical situations considered. For instance in kinematics I one sees that even in the case $\theta_e = 150^\circ$, where the various prescriptions give practically the same

results in the low p region and the RPWIA practically coincides with PWIA, the high p region ($300 < p < 500$ MeV) shows important relativistic effects whose size depends on the choice of the current operator.

We also point out that at high p the cross section is significantly higher for the CC1 choices. The results shown in fig. 12 reflect the behaviour observed in fig. 7. A detailed quantitative analyses of the role of the negative-energy projections on the differential cross sections for different current choices at any p -value and various kinematics observed in figs. 12–14 can also be performed using the results shown in figs. 1, 5 and 6.

5. Summary and final remarks

We have studied the relationship between relativistic and non-relativistic treatments of the plane-wave impulse approximation to $A(e,e'p)B$ reactions by inserting the completeness relation into the relativistic transition nuclear current. This allows one to separate the RPWIA differential cross section into contributions from positive-energy projections and from negative-energy projections of the bound nucleon wave function. This separation, exhibited in eq. (49), clearly demonstrates that the factorization limit of PWIA expressed by eq. (1) (see also eq. (45)) breaks down in RPWIA due to the presence of the negative-energy projection that although small is non-zero for a relativistic bound nucleon wave function. Typically, N_{uv} is one order of magnitude smaller than N_{uu} and N_{vv} is two orders of magnitude smaller for $p < 300$ MeV. This is so for the $1p_{1/2}$ shell in ^{16}O considered here, and we have observed a similar trend for various shells in different nuclei [25].

If we consider only the positive-energy projection of the relativistic bound nucleon wave function we recover the PWIA factorized expression that relates $A(e, e'p)B$ scattering to free electron-proton scattering through the elementary differential cross-section $\sigma^{ep} = \sigma_{uu}^{ep}$. However if we also take into account the negative-energy projection of the relativistic bound nucleon wave function other single-nucleon components σ_{uv}^{ep} and σ_{vv}^{ep} appear that are not present in the case of electron scattering from a free nucleon (or antinucleon). It is in this sense that we speak of lack of factorization in RPWIA. Obviously, the extent to which

factorization breaks down is measured by the relative importance of the contributions from the negative-energy projections.

We have studied the relative importance of these contributions with different choices of the current operators and of the kinematics. A quantitative study has been presented of —both single-nucleon and total— response functions and differential cross sections for different choices of the current operator and of the kinematics, focussing on the case of a $1p_{1/2}$ bound nucleon in ^{16}O . The main outcome of this study can be summarized as follows.

The role of the negative-energy component in the total differential cross section is to cause a reduction at low p ($p < 300$ MeV) and an increase at high p ($p \gtrsim 300$ MeV). This affects both the value of the spectroscopic factors and the shape of the extracted momentum distribution $\tilde{\rho}(p)$ [8, 9, 10].

The reduction at low p is generally small (less than a 15% for the NCC1, NCC2, CC1⁽⁰⁾ and CC2⁽⁰⁾ choices) and depends mainly on the kinematics. The largest reduction is found at small q values ($q < 500$ MeV) and at forward angles for the current choice CC1⁽³⁾. The sizeable difference at low p and q (forward angles) observed between the predictions of the CC1⁽⁰⁾ and CC1⁽³⁾ choices can be traced back to the difference between the longitudinal currents in eqs. (80,81), and it is also present in the positive-energy projections. Actually a sizeable difference at these kinematics is also observed between CC1⁽⁰⁾ and CC1⁽³⁾ results (as well as between CC2⁽⁰⁾ and CC2⁽³⁾ results) in the single-nucleon component σ_{uu} .

At low p , the positive-energy projections are dominant and the RPWIA results do not differ so much from the PWIA ones; however at $p > 300$ MeV the negative-energy projections play a more important role and the differences between current choices are enhanced. Indeed the single-nucleon components σ_{uv} and σ_{vv} in general depend much more on the choice of the current operator (CC1 or CC2) than does the positive-energy projection σ_{uu} and this is mainly seen in the total differential cross sections at high p .

As a general rule, the NCC2 and CC2⁽⁰⁾ choices minimize the effect of the negative-energy components, while all choices corresponding to the CC1 operator tend to enhance the contributions of the negative-energy components. The analyses of the nuclear current components in coordinate space show that, compared to CC2, the CC1 choices give more

weight to the dynamical enhancement of the lower components that appear multiplied by the *large* $S + V$ potential.

The response functions R^{TL} and R^{TT} are particularly sensitive to the combined effect of the negative-energy component and the choice of the current operator, because the cross term R_C^{TL} (R_C^{TT}) can be larger than the positive-energy projection R_P^{TL} (R_P^{TT}). As a net result one can find up to a factor of 3 difference between predictions of various current choices. While there is basically no difference between NCC2 and CC2⁽⁰⁾ predictions, the choices NCC1, CC1⁽⁰⁾ and CC2⁽³⁾ predict an R^{TL} response that is about 40% larger, and the CC1⁽³⁾ choice predicts a three times larger R^{TL} response. These large effects can be traced back to the difference between the CC1 and CC2 current operators in eq. (82). Clearly the $(\mathcal{P} - M)$ term that has no effect in the positive-energy projection R_P^{TL} has an important effect in the crossed terms R_C^{TL} and in the negative-energy term R_N^{TL} . Obviously the $(\mathcal{P} - M)$ term also causes differences between CC1 and CC2 predictions in the R_C and R_N terms of other response functions, but it is in the case of the TL and TT responses where the net effect is maximum because of the small values of the positive-energy projections.

The effect in R^{TL} is particularly interesting because this response can be more easily measured than R^{TT} and data on R^{TL} are already available. Whereas for most of the current prescriptions (NCC1, NCC2, CC1⁽⁰⁾ and CC2⁽⁰⁾) and at low p values ($p \lesssim 400$ MeV) the relativistic and non-relativistic results for the longitudinal and transverse responses differ at most by a 15%, in the case of the longitudinal-transverse (R^{TL}) response the relativistic prediction is at least a 50% larger than the non-relativistic one. It is important to point out that there is experimental evidence of the fact that a different spectroscopic factor is needed for the R^{TL} response than for the R^L and R^T ones. This experimental evidence follows from a non-relativistic analyses of the data [26, 27]. Although considering other effects such as two-body meson-exchange currents can explain part of this difference [28], it is clear that relativity plays a very important role in understanding this response, and it will be very interesting to see to what extent such discrepancies may be related to the relativistic effects found here [25].

Acknowledgements

This work is supported in part by a NATO Collaborative Research Grant Number 940183, in part by DGICYT (Spain) under Contract Nos. PB/95–0123 and PB/95–0533–A and in part by funds provided by the US Department of Energy (D.O.E.) under cooperative agreement #DE–FC01–94ER40818.

Appendix A

• Free Dirac Spinors

We follow the conventions of Bjorken and Drell [17]. In particular, the free Dirac spinors are

$$u(\mathbf{p}, s) = \sqrt{\frac{\bar{E} + M}{2M}} \begin{pmatrix} \chi^s \\ \frac{\boldsymbol{\sigma} \cdot \mathbf{p}}{\bar{E} + M} \chi^s \end{pmatrix} \quad (113)$$

$$v(\mathbf{p}, s) = \sqrt{\frac{\bar{E} + M}{2M}} \begin{pmatrix} \frac{\boldsymbol{\sigma} \cdot \mathbf{p}}{\bar{E} + M} \chi^s \\ \chi^s \end{pmatrix} \quad (114)$$

where \bar{E} denotes $\bar{E} = \sqrt{M^2 + \mathbf{p}^2}$.

1. Normalization

$$\bar{u}(\mathbf{p}, s)u(\mathbf{p}, s) = -\bar{v}(\mathbf{p}, s)v(\mathbf{p}, s) = 1 \quad . \quad (115)$$

2. Completeness relation

$$\sum_s [u_\alpha(\mathbf{p}, s)\bar{u}_\beta(\mathbf{p}, s) - v_\alpha(\mathbf{p}, s)\bar{v}_\beta(\mathbf{p}, s)] = \delta_{\alpha\beta} \quad . \quad (116)$$

• Relativistic Bound Nucleon Wave Function

The relativistic wave function for the bound nucleon in momentum space is given by

$$\Psi_\kappa^m(\mathbf{p}) = \frac{1}{(2\pi)^{3/2}} \int d\mathbf{r} e^{-i\mathbf{p} \cdot \mathbf{r}} \Psi_\kappa^m(\mathbf{r}) = (-i)^\ell \begin{pmatrix} g_\kappa(p) \\ S_\kappa f_\kappa(p) \frac{\boldsymbol{\sigma} \cdot \mathbf{p}}{p} \end{pmatrix} \Phi_\kappa^m(\Omega_p) \quad (117)$$

with $S_\kappa = \kappa/|\kappa|$, $j = |\kappa| - \frac{1}{2}$ and the quantum number ℓ given by the relation

$$\ell = \begin{cases} \kappa & \text{for } \kappa > 0 \\ -\kappa - 1 & \text{for } \kappa < 0 \end{cases} \quad (118)$$

The function $\Phi_\kappa^m(\Omega_p)$ is given by

$$\Phi_\kappa^m(\Omega_p) = \langle \hat{p} | \ell \frac{1}{2} j m \rangle = \sum_{\mu s} \langle \ell \mu \frac{1}{2} s | j m \rangle Y_\ell^\mu(\Omega_p) \chi^s = \sum_s \chi^s \langle s | \Phi_\kappa^m \rangle \quad (119)$$

and satisfies the relation

$$\Phi_{-\kappa}^m(\Omega_p) = -\frac{\boldsymbol{\sigma} \cdot \mathbf{p}}{p} \Phi_\kappa^m(\Omega_p) . \quad (120)$$

The radial functions g_κ and f_κ in momentum space are obtained from the respective functions in coordinate space

$$g_\kappa(p) = \sqrt{\frac{2}{\pi}} \int_0^\infty r^2 dr g_\kappa(r) j_\ell(pr) \quad (121)$$

$$f_\kappa(p) = \sqrt{\frac{2}{\pi}} \int_0^\infty r^2 dr f_\kappa(r) j_{\bar{\ell}}(pr) \quad (122)$$

with $j_\ell(pr)$ the Riccati–Bessel functions and $\ell = \kappa$, $\bar{\ell} = \kappa - 1$ for $\kappa > 0$; $\ell = |\kappa| - 1$, $\bar{\ell} = |\kappa|$ for $\kappa < 0$. The radial functions in coordinate space $g_\kappa(r)$ and $f_\kappa(r)$ satisfy the Dirac equation

$$\frac{df_\kappa}{dr} = \frac{\kappa - 1}{r} f_\kappa - [E - M - U_S - U_V] g_\kappa \quad (123)$$

$$\frac{dg_\kappa}{dr} = -\frac{\kappa - 1}{r} g_\kappa - [E - M + U_S - U_V] f_\kappa \quad (124)$$

with U_S (U_V) the scalar (vector) potentials that describe the target nucleus [12,13], and the normalization is

$$\int r^2 dr (g_\kappa^2(r) + f_\kappa^2(r)) = \int p^2 dp (g_\kappa^2(p) + f_\kappa^2(p)) = 1 . \quad (125)$$

Hence the relativistic (vector) density in momentum space normalized to 1 is

$$N_b^r(p) = \frac{1}{\hat{j}^2} \sum_m \Psi_\kappa^{m+} \Psi_\kappa^m = \frac{(g_\kappa^2(p) + f_\kappa^2(p))}{4\pi} . \quad (126)$$

Appendix B

In this appendix we present in detail the algebra needed in order to evaluate the positive and negative energy projection contributions to the hadronic tensor (see eq. (24)). Let us start with the contribution from the positive-energy projections. It is given by (for simplicity we suppress the index b on the bound proton wave function and quantum numbers)

$$\begin{aligned}
W_P^{\mu\nu} &\equiv \frac{2}{2j+1} \sum_m \sum_{s_N} \langle \hat{J}^\mu \rangle_u^* \langle \hat{J}^\nu \rangle_u \\
&= \frac{2}{2j+1} \sum_m \sum_{ss'} [\bar{u}(\mathbf{p}, s) \Psi_\kappa^m(\mathbf{p})]^* [\bar{u}(\mathbf{p}, s') \Psi_\kappa^m(\mathbf{p})] \\
&\times \sum_{s_N} [\bar{u}(\mathbf{p}_N, s_N) \hat{J}^\mu u(\mathbf{p}, s)]^* [\bar{u}(\mathbf{p}_N, s_N) \hat{J}^\nu u(\mathbf{p}, s')] . \quad (127)
\end{aligned}$$

Introducing the tensor $\mathcal{W}_{s's}^{\mu\nu}$ defined as

$$\mathcal{W}_{s's}^{\mu\nu} = \sum_{s_N} [\bar{u}(\mathbf{p}_N, s_N) \hat{J}^\mu u(\mathbf{p}, s)]^* [\bar{u}(\mathbf{p}_N, s_N) \hat{J}^\nu u(\mathbf{p}, s')] \quad (128)$$

and using the result obtained for the coefficient $[\bar{u}(\mathbf{p}, s) \Psi_\kappa^m(\mathbf{p})]$ as given in eq. (14), we can write

$$W_P^{\mu\nu} = \frac{2}{2j+1} \left(\frac{\bar{E} + M}{2M} \right) |\alpha_\kappa(p)|^2 \sum_{ss'} \mathcal{W}_{s's}^{\mu\nu} \sum_m \langle s | \Phi_\kappa^m \rangle^* \langle s' | \Phi_\kappa^m \rangle . \quad (129)$$

Now we can make use of the general relation given by eq. (28) to get the result shown in eq. (30).

In the case of the contribution from negative-energy projections, we have

$$\begin{aligned}
W_N^{\mu\nu} &\equiv \frac{2}{2j+1} \sum_m \sum_{s_N} \langle \hat{J}^\mu \rangle_v^* \langle \hat{J}^\nu \rangle_v \\
&= \frac{2}{2j+1} \sum_m \sum_{ss'} [\bar{v}(\mathbf{p}, s) \Psi_\kappa^m(\mathbf{p})]^* [\bar{v}(\mathbf{p}, s') \Psi_\kappa^m(\mathbf{p})] \\
&\times \sum_{s_N} [\bar{u}(\mathbf{p}_N, s_N) \hat{J}^\mu v(\mathbf{p}, s)]^* [\bar{u}(\mathbf{p}_N, s_N) \hat{J}^\nu v(\mathbf{p}, s')] . \quad (130)
\end{aligned}$$

Introducing the tensor $\mathcal{Z}_{s's}^{\mu\nu}$ given by

$$\mathcal{Z}_{s's}^{\mu\nu} = \sum_{s_N} [\bar{u}(\mathbf{p}_N, s_N) \hat{J}^\mu v(\mathbf{p}, s)]^* [\bar{u}(\mathbf{p}_N, s_N) \hat{J}^\nu v(\mathbf{p}, s')] \quad (131)$$

and using the results given by eqs. (15,120), we can write

$$\begin{aligned}
W_N^{\mu\nu} &= \frac{2}{2j+1} \left(\frac{\bar{E} + M}{2M} \right) |\beta_\kappa(p)|^2 \sum_{ss'} \mathcal{Z}_{s's}^{\mu\nu} \sum_m \langle s | \Phi_{-\kappa}^m \rangle^* \langle s' | \Phi_{-\kappa}^m \rangle \\
&= \frac{2}{2j+1} \left(\frac{\bar{E} + M}{2M} \right) |\beta_\kappa(p)|^2 \frac{1}{p^2} \sum_{ss'} \mathcal{Z}_{s's}^{\mu\nu} \\
&\quad \times \sum_{\delta\delta'} [\chi_s^+(\boldsymbol{\sigma} \cdot \mathbf{p}) \chi^\delta]^\dagger [\chi_{s'}^+(\boldsymbol{\sigma} \cdot \mathbf{p}) \chi^{\delta'}] \sum_m \langle \delta | \Phi_\kappa^m \rangle^* \langle \delta' | \Phi_\kappa^m \rangle .
\end{aligned} \tag{132}$$

Using the relation given by eq. (28), we get

$$W_N^{\mu\nu} = \left(\frac{1}{8\pi} \right) \left(\frac{\bar{E} + M}{M} \right) |\beta_\kappa(p)|^2 \frac{1}{p^2} \sum_{ss'} \mathcal{Z}_{s's}^{\mu\nu} \sum_\delta [\chi_s^+(\boldsymbol{\sigma} \cdot \mathbf{p}) \chi^\delta]^\dagger [\chi_{s'}^+(\boldsymbol{\sigma} \cdot \mathbf{p}) \chi^\delta] , \tag{133}$$

where the sum over the index δ is simply

$$\sum_\delta [\chi_s^+(\boldsymbol{\sigma} \cdot \mathbf{p}) \chi^\delta]^\dagger [\chi_{s'}^+(\boldsymbol{\sigma} \cdot \mathbf{p}) \chi^\delta] = p^2 \delta_{ss'} \tag{134}$$

and the final result reduces to the expression given in eq. (31). Note that the single-nucleon tensor $\mathcal{Z}^{\mu\nu} \equiv \sum_s \mathcal{Z}_{ss}^{\mu\nu}$ can be easily calculated using trace techniques (eq. (39).)

Let us proceed now to the evaluation of the cross term containing products of both positive and negative energy projections. Proceeding as in the previous cases and using eq. (29) we can write

$$\begin{aligned}
W_C^{\mu\nu} &= \frac{-2}{2j+1} \sum_m \sum_{s_N} (\langle \hat{J}^\mu \rangle_u^* \langle \hat{J}^\nu \rangle_v + \langle \hat{J}^\mu \rangle_v^* \langle \hat{J}^\nu \rangle_u) \\
&= \left(\frac{1}{8\pi} \right) \left(\frac{\bar{E} + M}{M} \right) \alpha_\kappa(p) \beta_\kappa(p) \frac{1}{p} \sum_{ss'} (\mathcal{I}_{s's}^{\mu\nu} + \mathcal{I}_{s's'}^{\nu\mu*}) [\chi_{s'}^+(\boldsymbol{\sigma} \cdot \mathbf{p}) \chi^s] ,
\end{aligned} \tag{135}$$

where we have introduced a new single-nucleon tensor defined as follows,

$$\mathcal{I}_{s's}^{\mu\nu} = \sum_{s_N} [\bar{u}(\mathbf{p}_N, s_N) \hat{J}^\mu u(\mathbf{p}, s)]^\dagger [\bar{u}(\mathbf{p}_N, s_N) \hat{J}^\nu v(\mathbf{p}, s')] . \tag{136}$$

From general properties of the γ matrices and making use of the trace techniques [17], we can express the tensor $\mathcal{I}_{s's}^{\mu\nu}$ as

$$\mathcal{I}_{s's}^{\mu\nu} = \frac{1}{8M^2} \text{Tr} \left\{ \gamma_5 (\not{P} + M) (\delta_{ss'} + \gamma_5 \not{\varphi}_{s's'}) \bar{\mathcal{J}}^\mu (\not{P}_N + M) J^\nu \right\} , \tag{137}$$

where the pseudovector $\varphi_{s's'}^\mu$ (see ref. [20] for details) reduces to the four-spin of the bound nucleon S_L^μ in the diagonal case, $s' = s$.

It is clear from the above expression that the off-diagonal contributions are purely symmetric and therefore one may write

$$\mathcal{I}_{s's}^{\mu\nu} = \mathcal{S}_{s's}^{\mu\nu} + i\delta_{ss'}\mathcal{A}^{\mu\nu} \ , \quad (138)$$

where $\mathcal{A}^{\mu\nu}$ is antisymmetric under $\mu \leftrightarrow \nu$ and real, whereas $\mathcal{S}_{s's}^{\mu\nu}$ is symmetric under $\mu \leftrightarrow \nu$, real for diagonal terms and in general complex for off-diagonal terms. These properties combined with the relation

$$\left[\chi_s^+(\boldsymbol{\sigma} \cdot \mathbf{p})\chi^s\right] = -\left[\chi_{-s}^+(\boldsymbol{\sigma} \cdot \mathbf{p})\chi^{-s}\right] \quad (139)$$

allow one to write finally,

$$W_C^{\mu\nu} = \left(\frac{-1}{8\pi}\right) \left(\frac{\bar{E} + M}{M}\right) \alpha_\kappa(p)\beta_\kappa(p) \sum_{ss'} \mathcal{R}_{s's}^{\mu\nu} \left[\chi_{s'}^+\left(\frac{\boldsymbol{\sigma} \cdot \mathbf{p}}{p}\right)\chi^s\right] \quad (140)$$

with

$$\mathcal{R}_{s's}^{\mu\nu} = \frac{1}{4M} \text{Tr} \left[\phi_{s's} \bar{J}^\mu (\not{P}_N + M) J^\nu \right] \ . \quad (141)$$

It can be proved that $\sum_{ss'} \mathcal{R}_{s's}^{\mu\nu} \left[\chi_{s'}^+\left(\frac{\boldsymbol{\sigma} \cdot \mathbf{p}}{p}\right)\chi^s\right]$ is just a trace and can be simply written as

$$\sum_{ss'} \mathcal{R}_{s's}^{\mu\nu} \left[\chi_{s'}^+\left(\frac{\boldsymbol{\sigma} \cdot \mathbf{p}}{p}\right)\chi^s\right] = \text{Tr} \left[\bar{J}^\mu \left(\frac{\not{P}_N + M}{2M}\right) J^\nu \gamma^0 \frac{\boldsymbol{\gamma} \cdot \mathbf{p}}{p} \frac{\not{P}}{M} \right] = 2\mathcal{N}^{\mu\nu} \quad (142)$$

with the tensor $\mathcal{N}^{\mu\nu}$ as introduced in section 2.3 (see eq. (40)).

Appendix C

In this appendix we give the explicit expressions of the single-nucleon tensors $\mathcal{W}^{\mu\nu}$, $\mathcal{Z}^{\mu\nu}$ and $\mathcal{R}^{\mu\nu}$ for the two current operators CC1 and CC2 in eqs. (65,66).

The following expressions for the various single-nucleon tensors are obtained:

- with \hat{J}_{CC1}^μ current operator

$$\begin{aligned} M^2\mathcal{W}^{\mu\nu} &= (F_1 + F_2)^2 \left(\bar{P}^\mu P_N^\nu + \bar{P}^\nu P_N^\mu + \frac{\bar{Q}^2}{2} g^{\mu\nu} \right) \\ &- \left[F_2(F_1 + F_2) - F_2^2 \left(\frac{1}{2} - \frac{\bar{Q}^2}{8M^2} \right) \right] (\bar{P} + P_N)^\mu (\bar{P} + P_N)^\nu \end{aligned} \quad (143)$$

$$\begin{aligned}
M^2 \mathcal{Z}^{\mu\nu} &= (F_1 + F_2)^2 \left(\bar{P}^\mu P_N^\nu + \bar{P}^\nu P_N^\mu - \frac{(\bar{P} + P_N)^2}{2} g^{\mu\nu} \right) \\
&- \frac{F_2^2}{8M^2} \bar{Q}^2 (\bar{P} + P_N)^\mu (\bar{P} + P_N)^\nu + F_2(F_1 + F_2) \left(P_N^\mu P_N^\nu - \bar{P}^\nu \bar{P}^\mu \right) \quad (144)
\end{aligned}$$

$$\begin{aligned}
M\mathcal{R}^{\mu\nu} &= (F_1 + F_2)^2 (S_L^\mu P_N^\nu + S_L^\nu P_N^\mu - P_N \cdot S_L g^{\mu\nu}) \\
&+ \frac{F_2^2}{4M^2} P_N \cdot S_L (\bar{P} + P_N)^\mu (\bar{P} + P_N)^\nu \\
&- \frac{F_2}{2} (F_1 + F_2) \left(S_L^\mu (\bar{P} + P_N)^\nu + S_L^\nu (\bar{P} + P_N)^\mu \right) \quad (145)
\end{aligned}$$

- with \hat{J}_{CC2}^μ current operator

$$\begin{aligned}
M^2 \mathcal{W}^{\mu\nu} &= F_1^2 \left(\bar{P}^\mu P_N^\nu + \bar{P}^\nu P_N^\mu + \frac{\bar{Q}^2}{2} g^{\mu\nu} \right) + F_1 F_2 \left(Q \cdot \bar{Q} g^{\mu\nu} - \frac{\bar{Q}^\mu Q^\nu + \bar{Q}^\nu Q^\mu}{2} \right) \\
&+ \frac{F_2^2}{4M^2} \left[P_N \cdot Q (\bar{P}^\mu Q^\nu + \bar{P}^\nu Q^\mu) + \bar{P} \cdot Q (P_N^\mu Q^\nu + P_N^\nu Q^\mu) \right. \\
&- Q^2 (P_N^\mu \bar{P}^\nu + P_N^\nu \bar{P}^\mu) - \left(2M^2 - \frac{\bar{Q}^2}{2} \right) Q^\mu Q^\nu \\
&\left. + g^{\mu\nu} \left(2M^2 Q^2 - \frac{Q^2 \bar{Q}^2}{2} - 2P_N \cdot Q \bar{P} \cdot Q \right) \right] \quad (146)
\end{aligned}$$

$$\begin{aligned}
M^2 \mathcal{Z}^{\mu\nu} &= F_1^2 \left(\bar{P}^\mu P_N^\nu + \bar{P}^\nu P_N^\mu - \frac{(\bar{P} + P_N)^2}{2} g^{\mu\nu} \right) \\
&+ F_1 F_2 \left(\frac{Q^\mu (\bar{P} + P_N)^\nu + Q^\nu (\bar{P} + P_N)^\mu}{2} - Q \cdot (\bar{P} + P_N) g^{\mu\nu} \right) \\
&+ \frac{F_2^2}{4M^2} \left[P_N \cdot Q (\bar{P}^\mu Q^\nu + \bar{P}^\nu Q^\mu) + \bar{P} \cdot Q (P_N^\mu Q^\nu + P_N^\nu Q^\mu) \right. \\
&- Q^2 (P_N^\mu \bar{P}^\nu + P_N^\nu \bar{P}^\mu) + \frac{\bar{Q}^2}{2} Q^\mu Q^\nu - g^{\mu\nu} \left(\frac{Q^2 \bar{Q}^2}{2} + 2P_N \cdot Q \bar{P} \cdot Q \right) \left. \right] \quad (147)
\end{aligned}$$

$$M\mathcal{R}^{\mu\nu} = F_1^2 (S_L^\mu P_N^\nu + S_L^\nu P_N^\mu - P_N \cdot S_L g^{\mu\nu})$$

$$\begin{aligned}
& + \frac{F_1 F_2}{2} (S_L^\mu Q^\nu + S_L^\nu Q^\mu - 2Q \cdot S_L g^{\mu\nu}) \\
& + \frac{F_2^2}{4M^2} \left[P_N \cdot Q (S_L^\mu Q^\nu + S_L^\nu Q^\mu) + S_L \cdot Q (P_N^\mu Q^\nu + P_N^\nu Q^\mu) \right. \\
& \left. - Q^2 (P_N^\mu S_L^\nu + P_N^\nu S_L^\mu) - P_N \cdot S_L Q^\mu Q^\nu + g^{\mu\nu} (Q^2 P_N \cdot S_L - 2P_N \cdot Q S_L \cdot Q) \right]
\end{aligned} \tag{148}$$

with $A \cdot B \equiv A_\mu B^\mu$.

Finally, we show in table I the components of the spin four-vector S_L^μ in the laboratory frame.

(θ_R, ϕ_R)	$\mu = 0$	$\mu = 1$	$\mu = 2$	$\mu = 3$
$(0, 0)$	χ'	$\frac{\chi\chi'}{\bar{\gamma}+1}$	0	$1 + \frac{\chi'^2}{\bar{\gamma}+1}$
$(\frac{\pi}{2}, 0)$	$\chi \cos \phi$	$(1 + \frac{\chi^2}{\bar{\gamma}+1}) \cos \phi$	$-\sin \phi$	$\frac{\chi\chi'}{\bar{\gamma}+1} \cos \phi$
$(\frac{\pi}{2}, \frac{\pi}{2})$	$\chi \sin \phi$	$(1 + \frac{\chi^2}{\bar{\gamma}+1}) \sin \phi$	$\cos \phi$	$\frac{\chi\chi'}{\bar{\gamma}+1} \sin \phi$

Table 1: Components of the spin four vector $S_L^\mu(\theta_R, \phi_R)$. The notation $\bar{\gamma} \equiv \frac{E}{M}$; $\chi \equiv \frac{p_N}{M} \sin \theta_N = \frac{p}{M} \sin \theta$; $\chi' \equiv \frac{p_N}{M} \cos \theta = \frac{p_N}{M} \cos \theta_N - 2\kappa$ and $\kappa \equiv \frac{q}{2M}$ has been introduced

References

- [1] See for instance S. Frullani and J. Mougey, **Adv. Nucl. Phys.** 14 (1985); T. de Forest, **Nucl. Phys. A** 132 (1969) 305; A.E.L. Dieperink and T. de Forest, **Ann. Rev. Nucl. Sci.** 25 (1975) 1.
- [2] P.K.A. de Witt Huberts, **J. Phys. G** 16 (1990) 507. L. Lapikás, **Nucl. Phys. A** 553 (1993) 297C. J.B. Lanen et al., **Nucl Phys. A** 560 (1993) 811. J. Wesseling et al., **Phys. Rev. C** 55 (1997) 2773.

- [3] E.N.M. Quint, Ph. D. Thesis, University of Amsterdam (1988).
- [4] I. Bobeldijk et al., **Phys. Rev. Lett.** 73 (1994) 2684.
- [5] V.R. Pandharipande, C.N. Papanicolas and J. Wambach, **Phys. Rev. Lett.** 53 (1984) 1133. Z.Y. Ma and J. Wambach, **Phys. Lett. B** 256 (1991) 1. C. Mahaux and R. Sartor, **Adv. Nucl. Phys.** 20 (1991) 1.
- [6] H. Müther and W.H. Dickhoff, **Phys. Rev. C** 49 (1994) R17.
- [7] J.P. McDermott, **Phys. Rev. Lett.** 65 (1990) 1991. Y. Jin, D.S. Onley and L.E. Wright, **Phys. Rev. C** 45 (1992) 1311.
- [8] J.M. Udías, P. Sarriguren, E. Moya de Guerra, E. Garrido and J.A. Caballero, **Phys. Rev. C** 48 (1993) 2731. J.M. Udías, Ph. D. Thesis, Universidad Autónoma de Madrid (1993).
- [9] J.M. Udías, P. Sarriguren, E. Moya de Guerra, E. Garrido and J.A. Caballero **Phys. Rev. C** 51 (1995) 3246.
- [10] J.M. Udías, P. Sarriguren, E. Moya de Guerra, and J.A. Caballero **Phys. Rev. C** 53 (1996) R1488.
- [11] S. Hama, B.C. Clark, E.D. Cooper, H.S. Sherif and R.L. Mercer, **Phys. Rev. C** 41 (1990) 2737. E.D. Cooper, S. Hama, B.C. Clark and R.L. Mercer, **Phys. Rev. C** 47 (1993) 297.
- [12] C.J. Horowitz, D.P. Murdock and B.D. Serot, in **Computational Nuclear Physics** (Eds. K. Langanke, J.A. Maruhn and S.E. Koonin), Springer-Verlag, Berlin (1991).
- [13] B.D. Serot and J.D. Walecka, **Adv. Nucl. Phys.** 16 (1986) 1.
- [14] Y. Jin and D.S. Onley, **Phys. Rev. C** 45 (1994) 377. M. Hedayati-Poor, J.I. Johansson and H.S. Sherif, **Phys. Rev. C** 51 (1995) 2044.
- [15] S.J. Brodsky, **Comm. Nucl. Part. Phys.** 12 (1984) 213. N. Thies, **Phys. Lett.** 166 B (1986) 23. E.D. Cooper and B.K. Jennings, **Nucl. Phys. A** 458 (1986) 717;

- G.E. Brown, W. Weise, G. Baym and J. Speth, Comments in Nucl. Part. Phys. **17** (1987) 39; S.J. Wallace, F. Gross and J.A. Tjon, **Phys. Rev. Lett.** **74** (1995) 228.
- [16] E. Garrido, J.A. Caballero, E. Moya de Guerra, P. Sarriguren and J.M. Udías, Nucl. Phys. **A584** (1995) 256.
- [17] J.D. Bjorken and S.D. Drell, RELATIVISTIC QUANTUM MECHANICS, McGraw-Hill, N.Y. (1964).
- [18] A.S. Raskin and T.W. Donnelly, Ann. Phys. **191** (1989) 78.
- [19] J.A. Caballero, E. Garrido, E. Moya de Guerra, P. Sarriguren and J.M. Udías, Ann. of Phys. **239** (1995) 351.
- [20] J.A. Caballero, T.W. Donnelly, and G. Poulis, Nucl. Phys. **A555** (1993) 709.
- [21] T. de Forest, Nucl. Phys. **A392** (1983) 232.
- [22] H.W.L. Naus, S.J. Pollock, J.H. Koch and U. Oelfke, Nucl. Phys. **A509** (1990) 717; S. Pollock, H.W.L. Naus and J.H. Koch, Phys. Rev. **C53** (1996) 2304.
- [23] C.J. Horowitz and B.D. Serot, Nucl. Phys. **A368**, (1981) 503; Phys. Lett. B **86**, (1979) 146.
- [24] F. Gross and D.O. Riska, Phys. Rev. **C36** (1987) 1928.
- [25] J.A. Caballero, E. Moya de Guerra, T.W. Donnelly and J.M. Udías, *work in progress*.
- [26] G.M. Spaltro *et al.*, Phys. Rev. C **48** (1993) 2385.
- [27] H.J. Bulten, Ph. D. thesis, University of Utrech (1992). L. Lapikás, Nucl. Phys. A **553** (1993) 297c.
- [28] V. van der Sluys, J. Ryckebush and M. Waroquier, Phys. Rev. C **49** (1994) 2695.

Figure captions

Figure 1: Left panel: projection components of the momentum distribution (in units of fm^3): $N_{uu}(p)$ (solid), $N_{uv}(p)$ (dotted) and $N_{vv}(p)$ (dashed). Right panel: $N_{uu}(p)$ (solid), $N_{uu}^{(0)}(p)$ (dotted) and $N_{uu}^{n.r.}(p)$ (dashed) (see text for details).

Figure 2a: Projection components of the single-nucleon response functions, \mathcal{R}_{uu}^K , \mathcal{R}_{uv}^K and \mathcal{R}_{vv}^K . Kinematics I have been chosen and results for the pure longitudinal (top) and interference longitudinal-transverse (bottom) responses are shown. Thick lines correspond to prescriptions that use the CC2 current operator and thin lines correspond to the CC1 operator. Prescriptions shown are: NCC2 (NCC1) (solid lines), CC2⁽⁰⁾ (CC1⁽⁰⁾) (short-dash lines) and CC2⁽³⁾ (CC1⁽³⁾) (long-dash lines).

Figure 2b: Same as fig. 2a, except that now for the pure transverse (top) and transverse-transverse interference (bottom) single-nucleon responses. Note that here all CC2 (CC1) prescriptions collapse into a single thick (thin) solid curve.

Figure 3a: Same as fig. 2a, except that now for kinematics II (see text).

Figure 3b: Same as fig. 2b, except that now for kinematics II (see text).

Figure 4a: Same as fig. 2a, except that now for kinematics III (see text).

Figure 4b: Same as fig. 2b, except that now for kinematics III (see text).

Figure 5: Projections of the single-proton cross section as given by eqs. (46-48). Results correspond to kinematics I and $\phi_N = 0^0$ (in-plane). Forward-angle electron scattering ($\theta_e = 30^0$) (top panel) and backward ($\theta_e = 150^0$) (bottom) have been chosen here. The labels are as in fig. 2a.

Figure 6: Same as fig. 5, except now for kinematics II and forward-angle electron scattering ($\theta_e = 12.5^0$).

Figure 7: Hadronic response functions for the $1p_{1/2}$ shell in ^{16}O and kinematics I. The labels of the various curves are as in fig. 2a. Note that for the two pure transverse responses,

R^T and R^{TT} , all the CC2 (CC1) prescriptions collapse into a single solid (dashed) curve.

Figure 8: Components of the nuclear responses, R_P^K , R_C^K and R_N^K (see eqs. (61–64)). Results are shown for longitudinal (top panel) and transverse-longitudinal interference (bottom panel) response functions. The rest of labeling is as in fig. 2a.

Figure 9: Same as fig. 8, except that now for the transverse (top) and transverse-transverse interference (bottom) responses.

Figure 10: Hadronic response functions for the $1p_{1/2}$ shell in ^{16}O and kinematics I. All of the results correspond to the prescription $\text{CC1}^{(0)}$. For each response we compare the fully relativistic result (solid) with the three components as introduced by eqs. (62–64): R_P^K (dotted), R_C^K (dashed) and R_N^K (long-dash). Some of the curves are multiplied by different scale factors.

Figure 11: Same as fig. 10, except that now the prescription $\text{CC2}^{(0)}$ has been chosen.

Figure 12: Differential cross section for the $1p_{1/2}$ shell in ^{16}O . Kinematics I have been chosen and results are presented for forward and backward electron scattering angles: $\theta_e = 30^\circ$ (left panel) and $\theta_e = 150^\circ$ (right panel). We show the fully relativistic results given by the prescriptions (see text): $\text{CC2}^{(0)}$ (thick-solid), $\text{CC1}^{(0)}$ (thin-solid), $\text{CC2}^{(3)}$ (thick-dash) and $\text{CC1}^{(3)}$ (thin-dash). We also show the results corresponding to the non-relativistic PWIA limit (dotted line) (see text for details).

Figure 13: Same as fig. 12, except that now for kinematics II and forward scattering angle ($\theta_e = 12.5^\circ$).

Figure 14: Same as fig. 12, except that now for kinematics III.

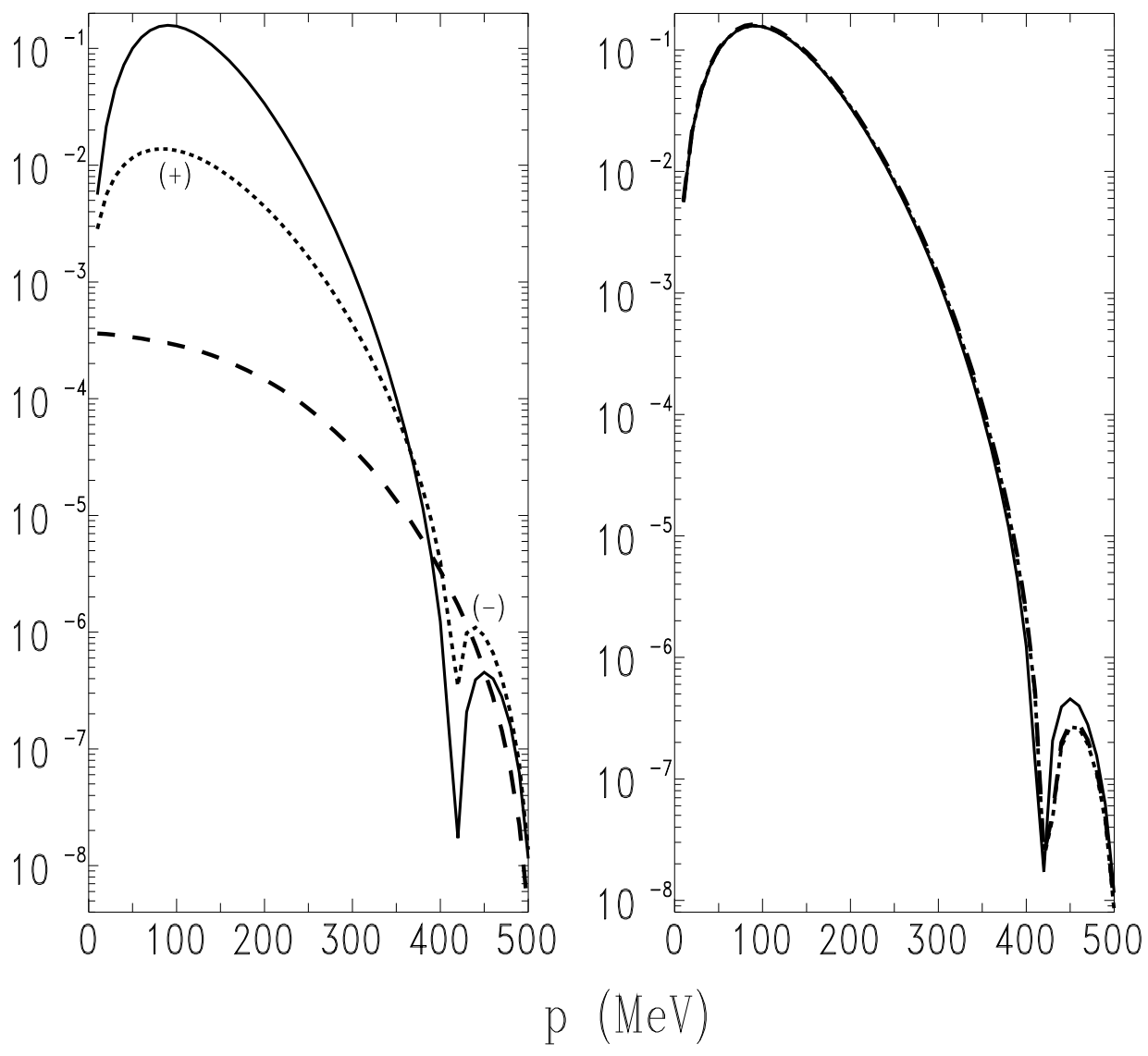


Figure 1

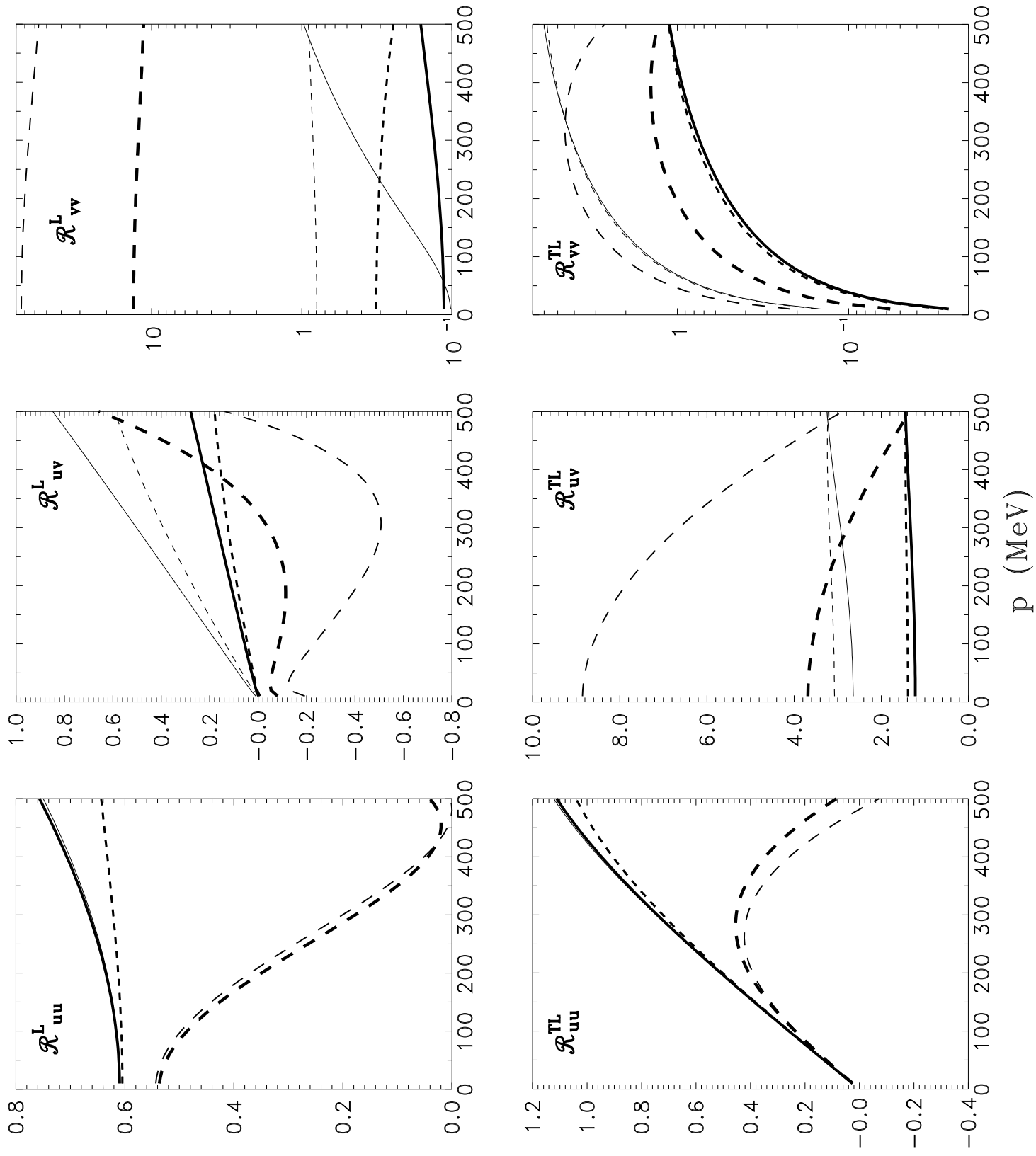


Figure 2a

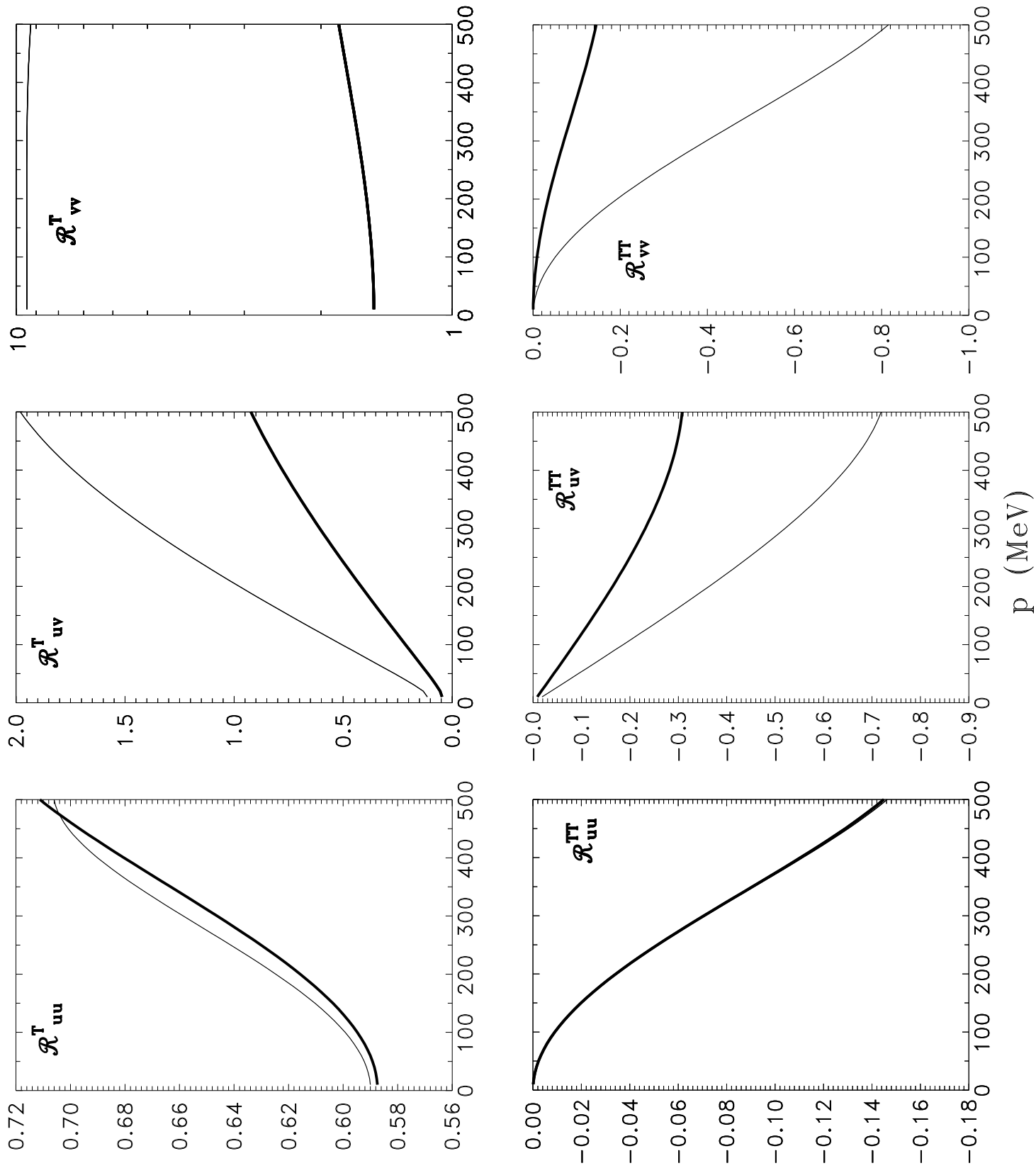


Figure 2b

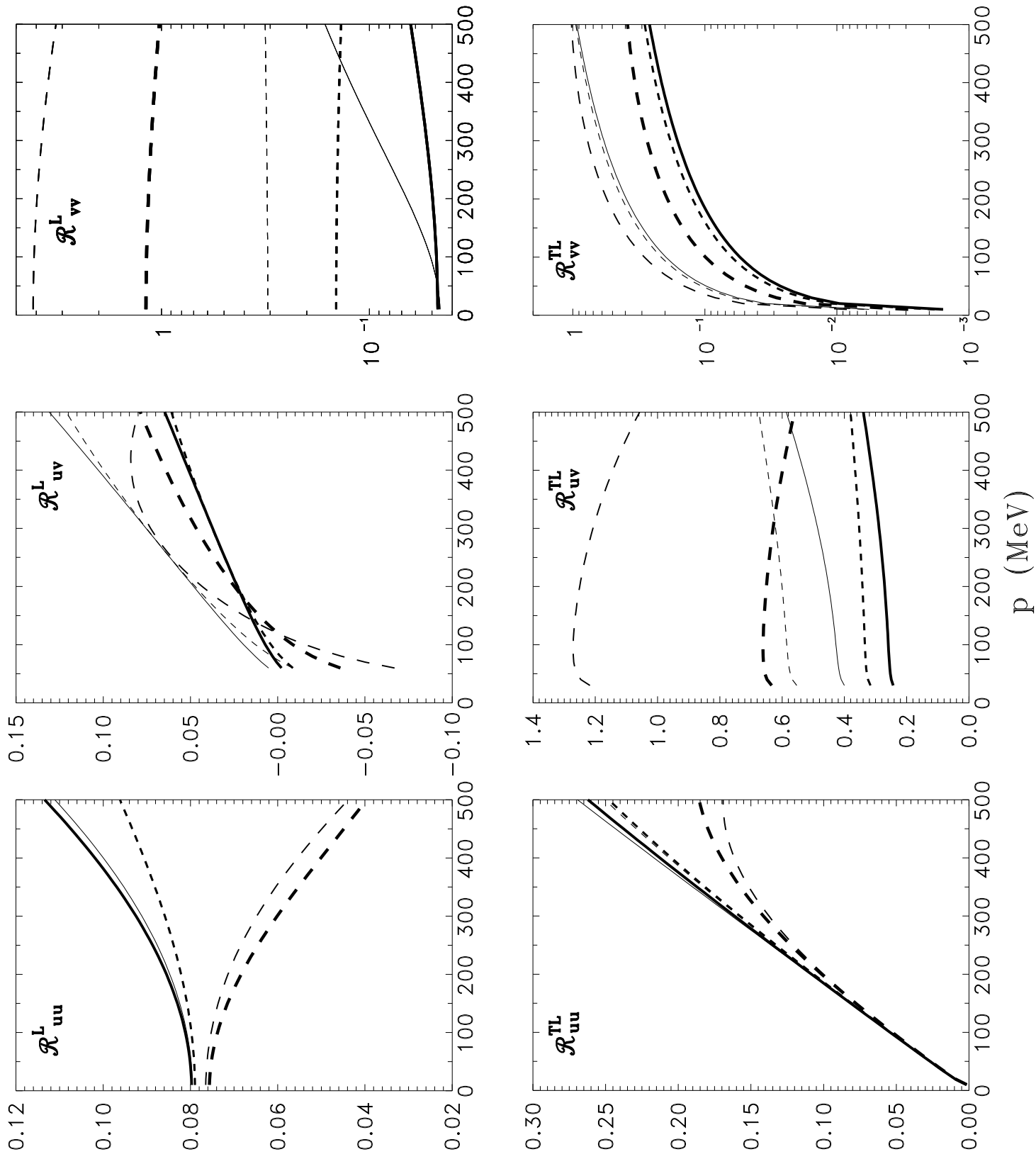


Figure 3a

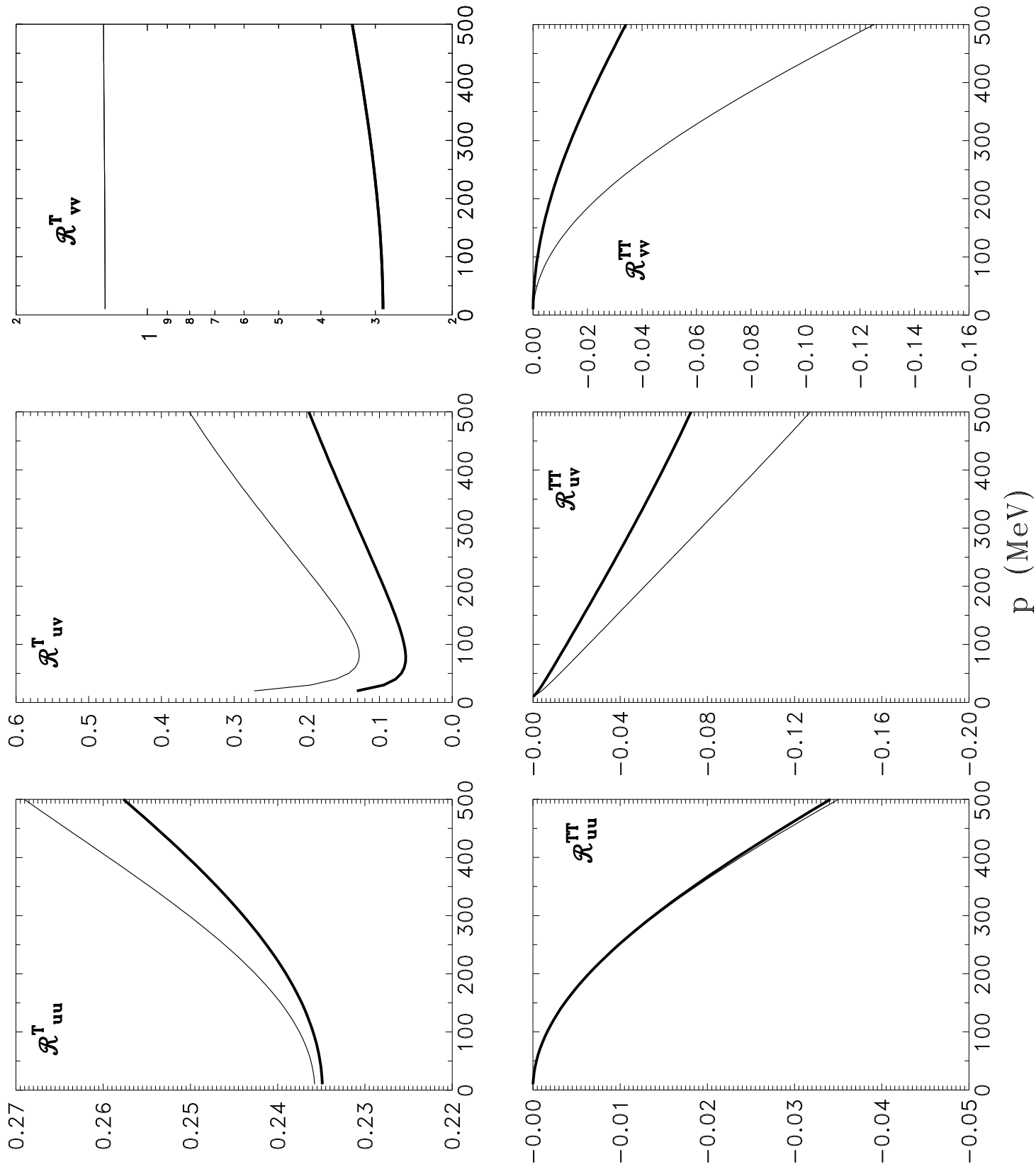


Figure 3b

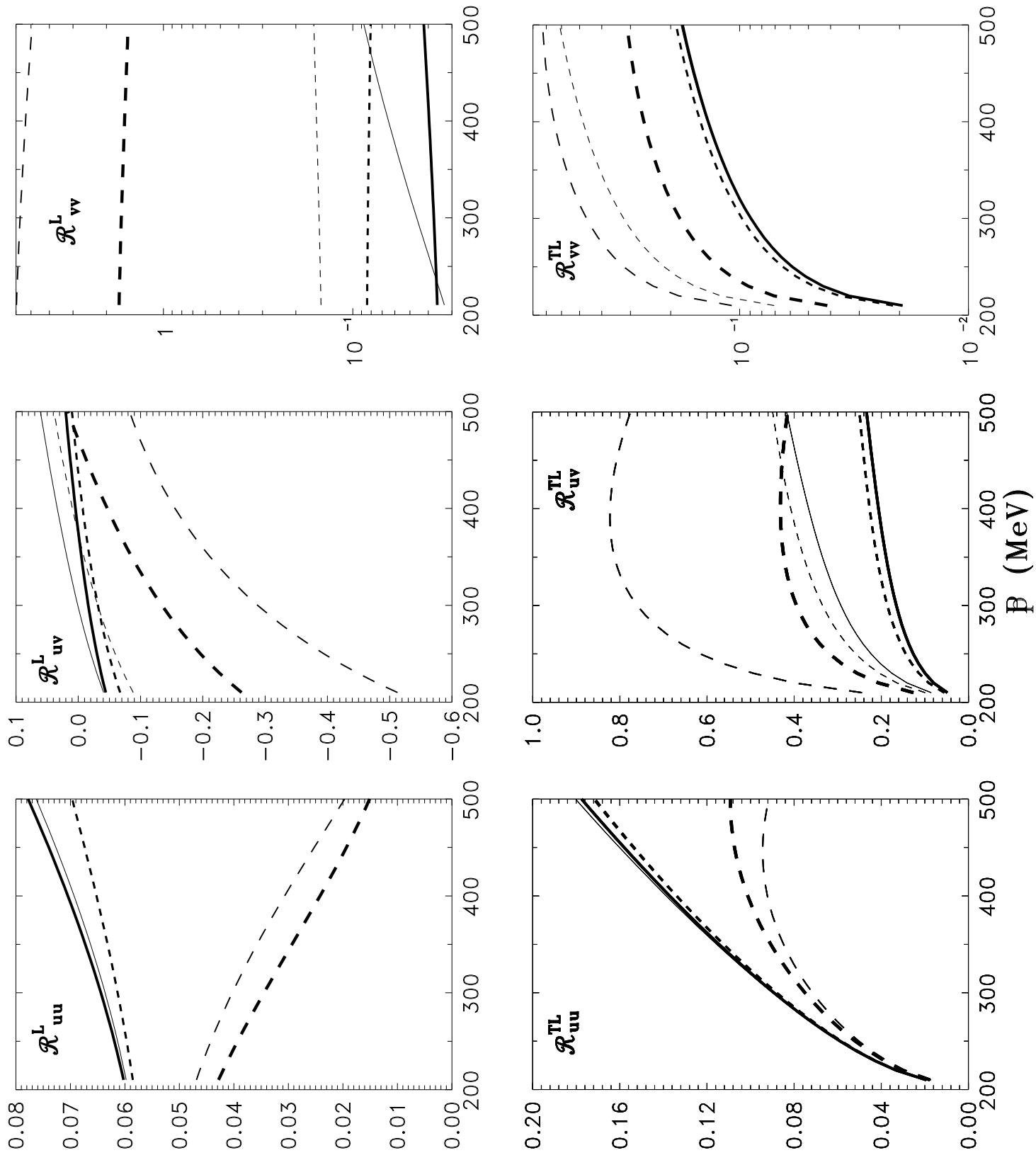


Figure 4a

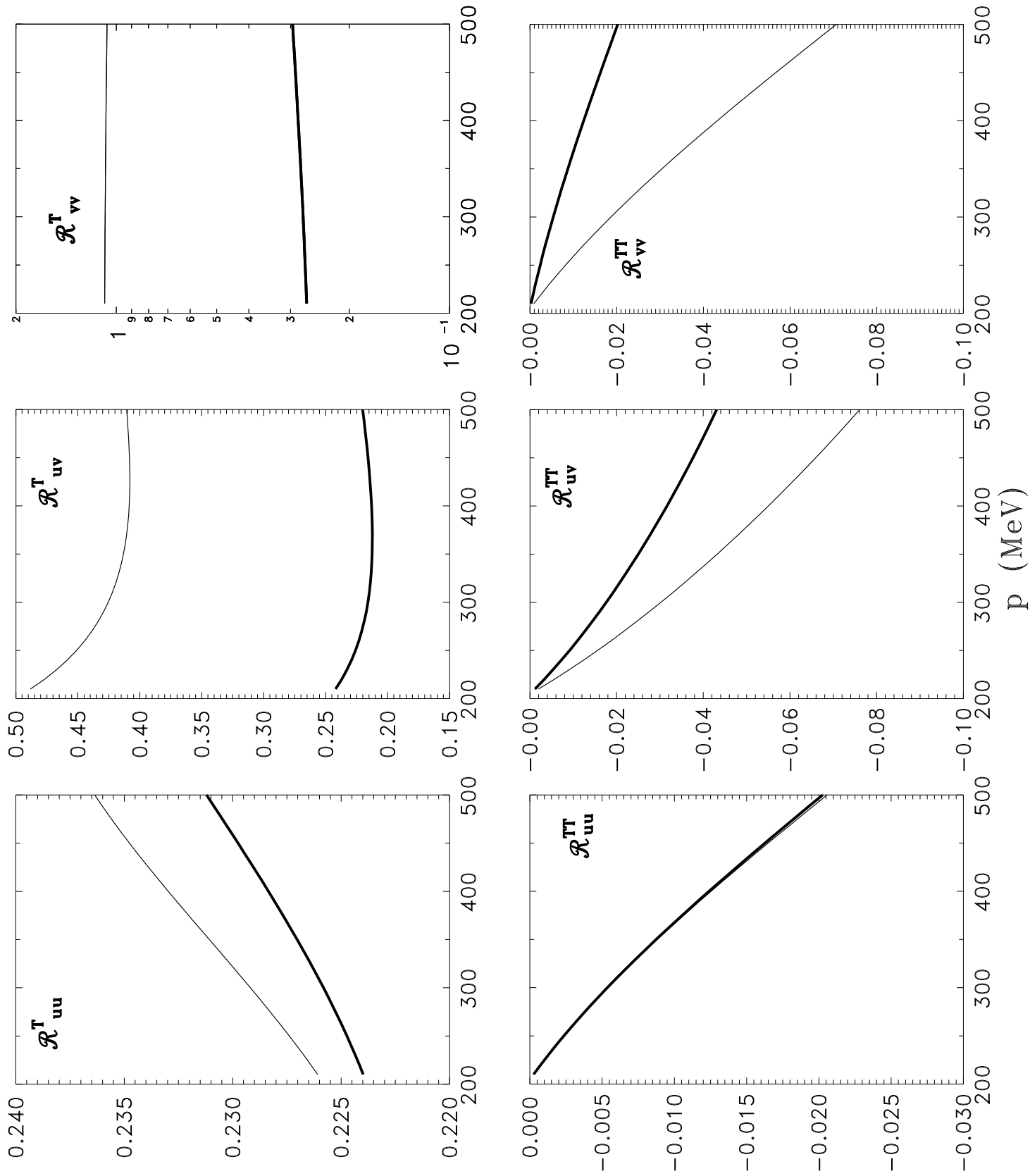


Figure 4b

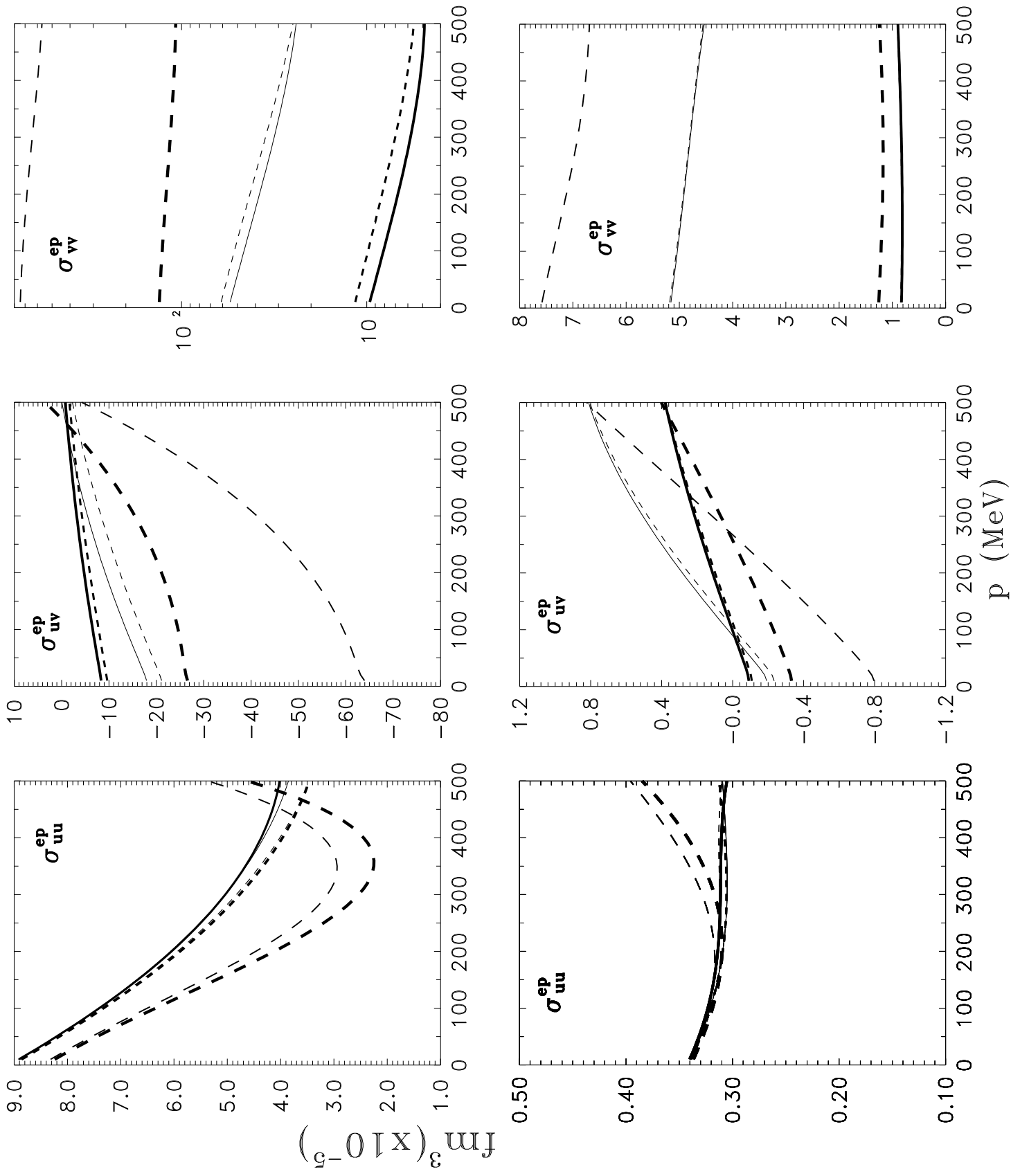


Figure 5

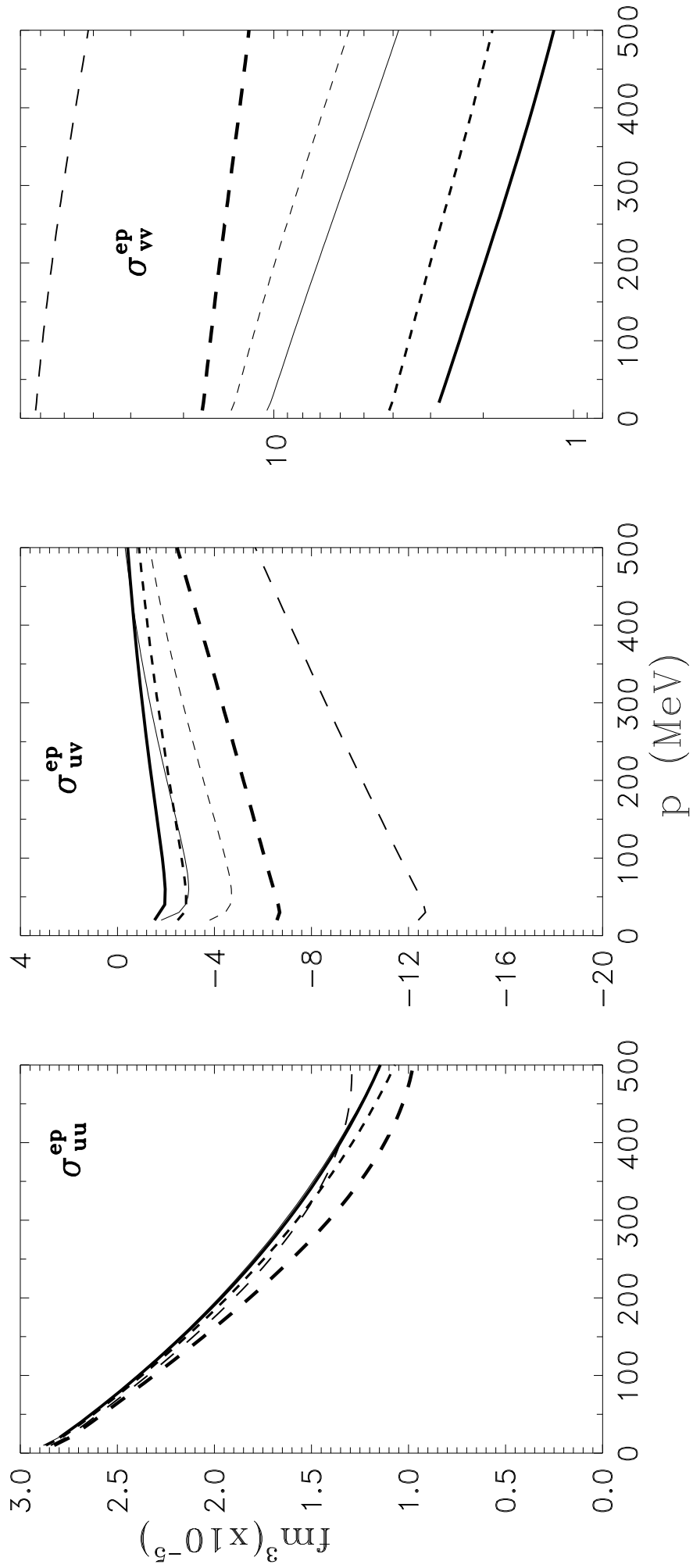


Figure 6

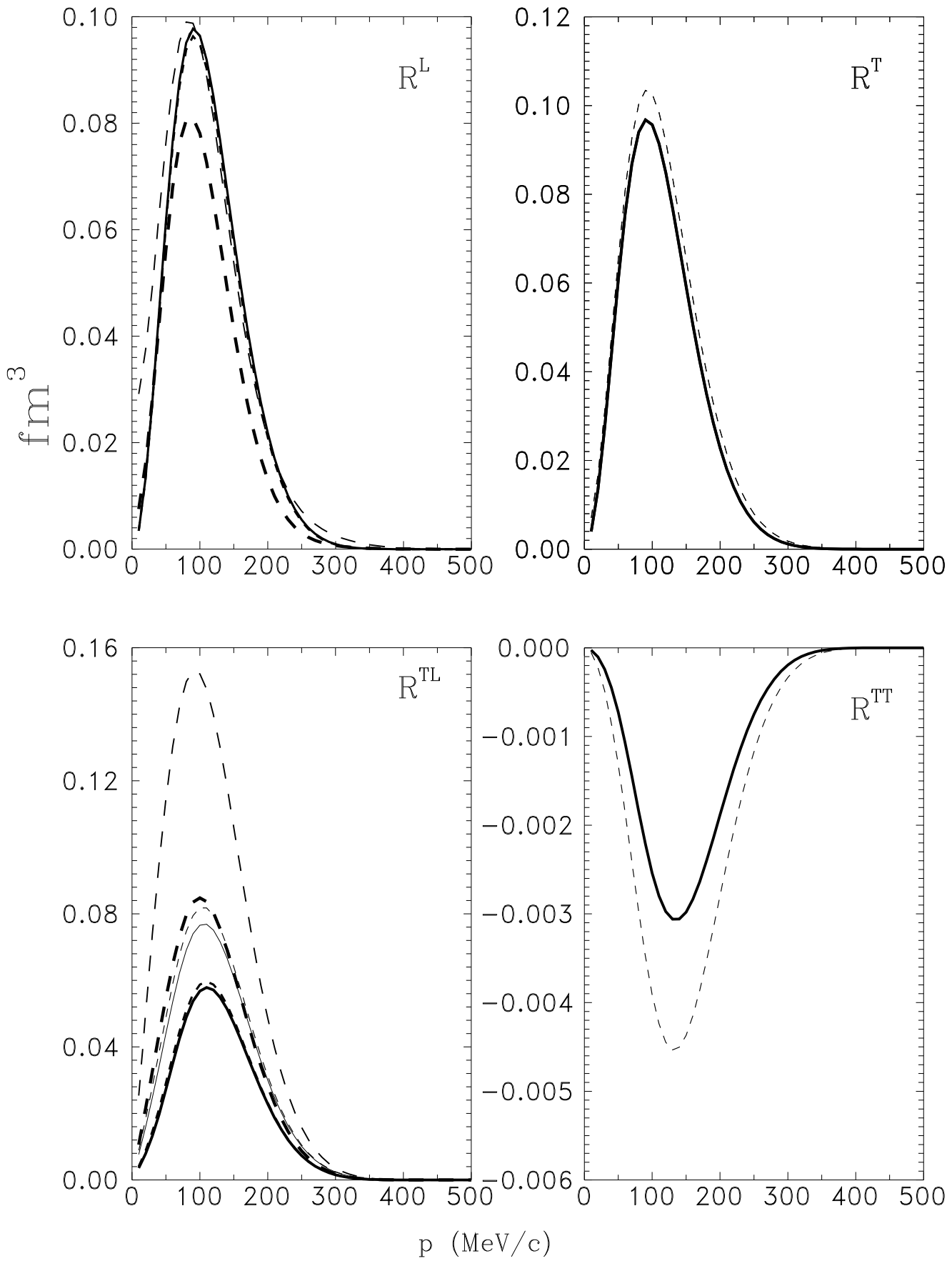


Figure 7

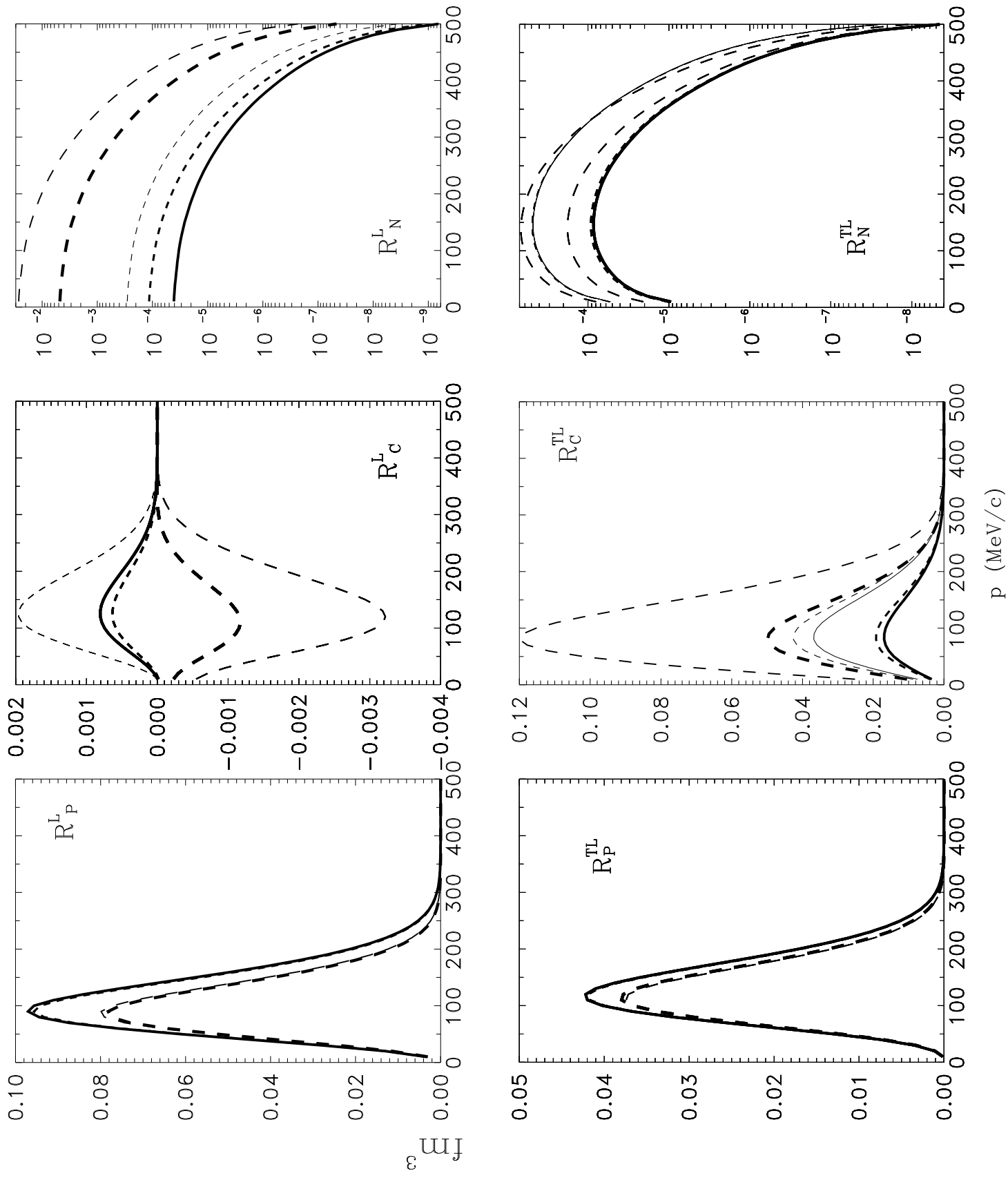


Figure 8

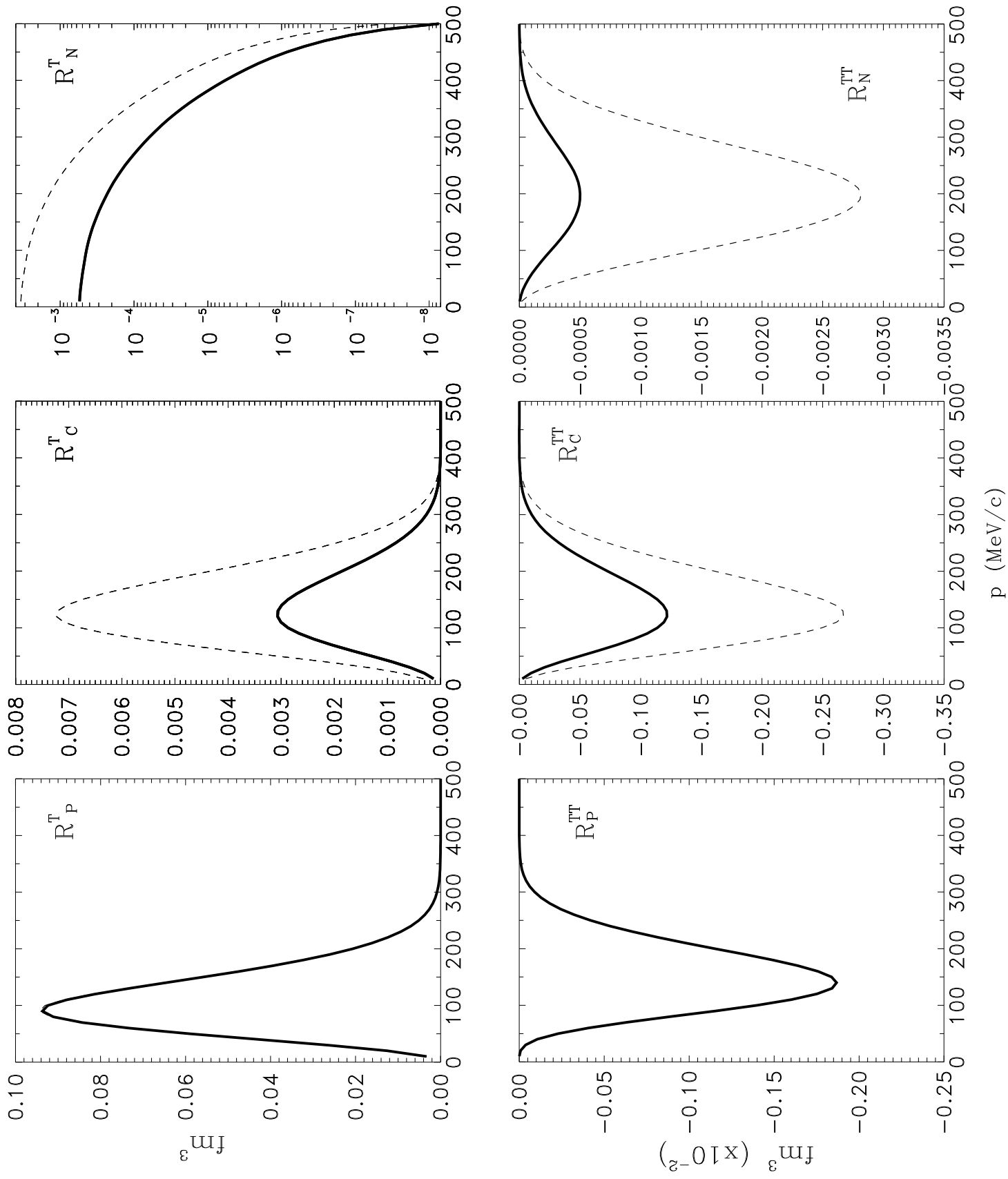


Figure 9

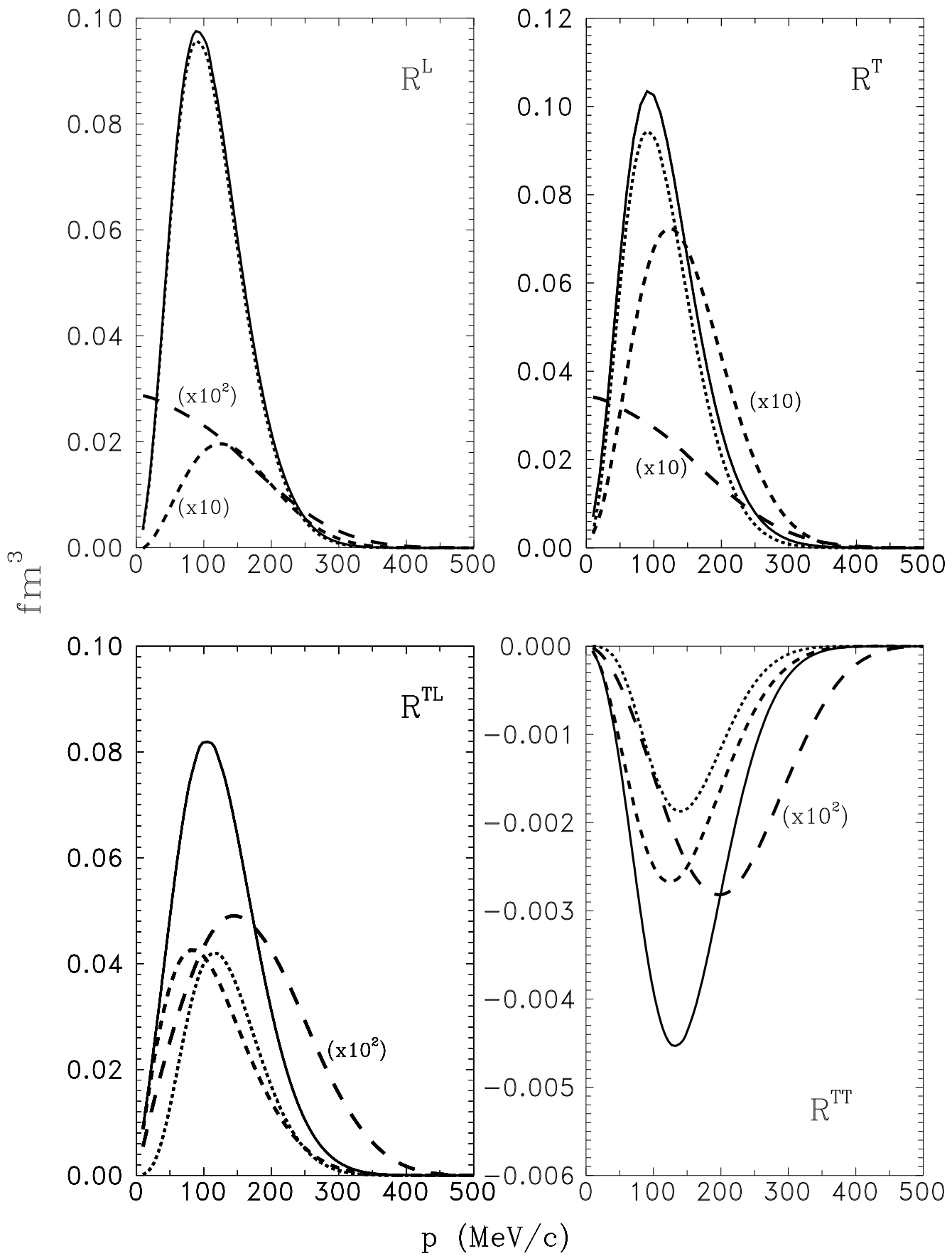


Figure 10

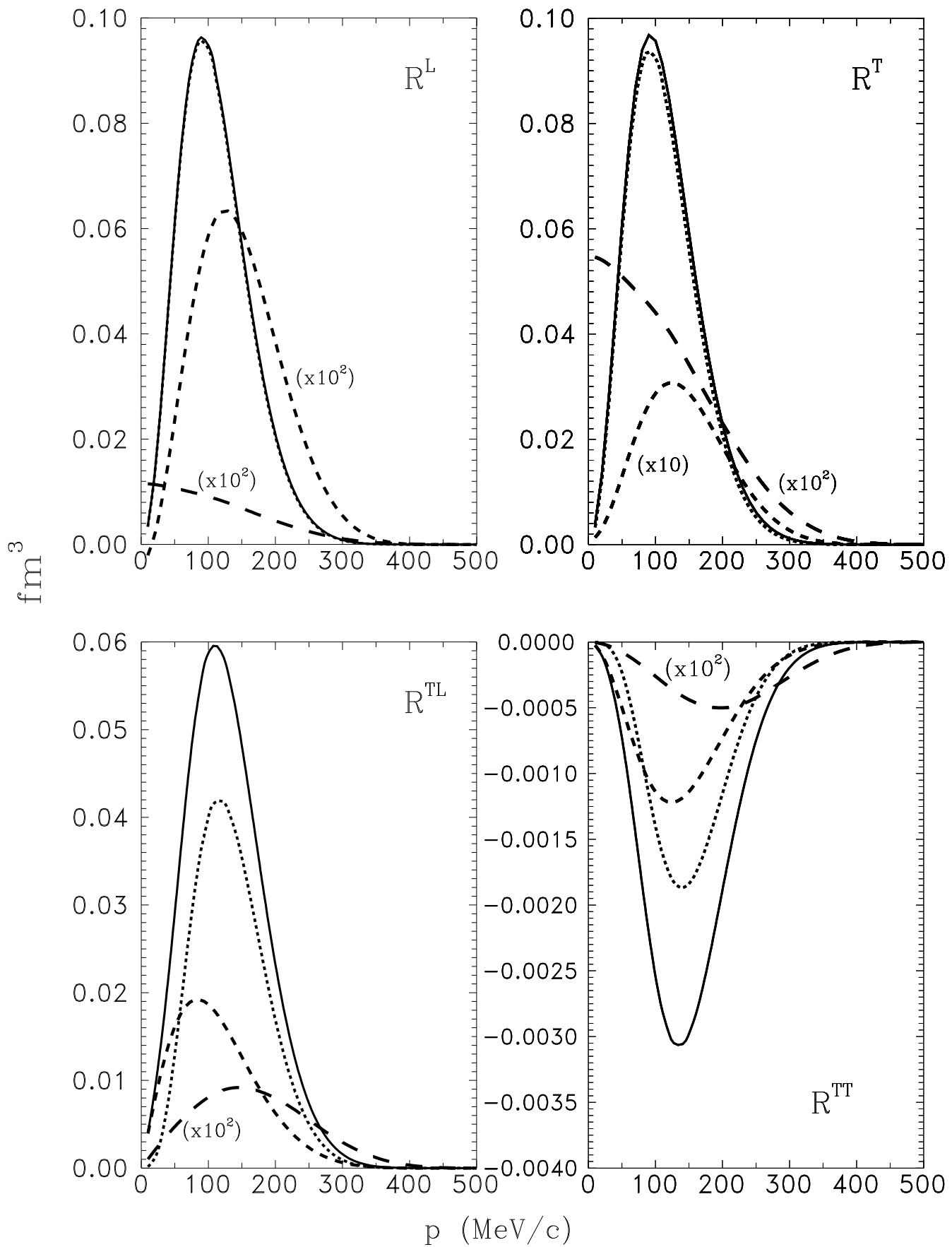


Figure 11

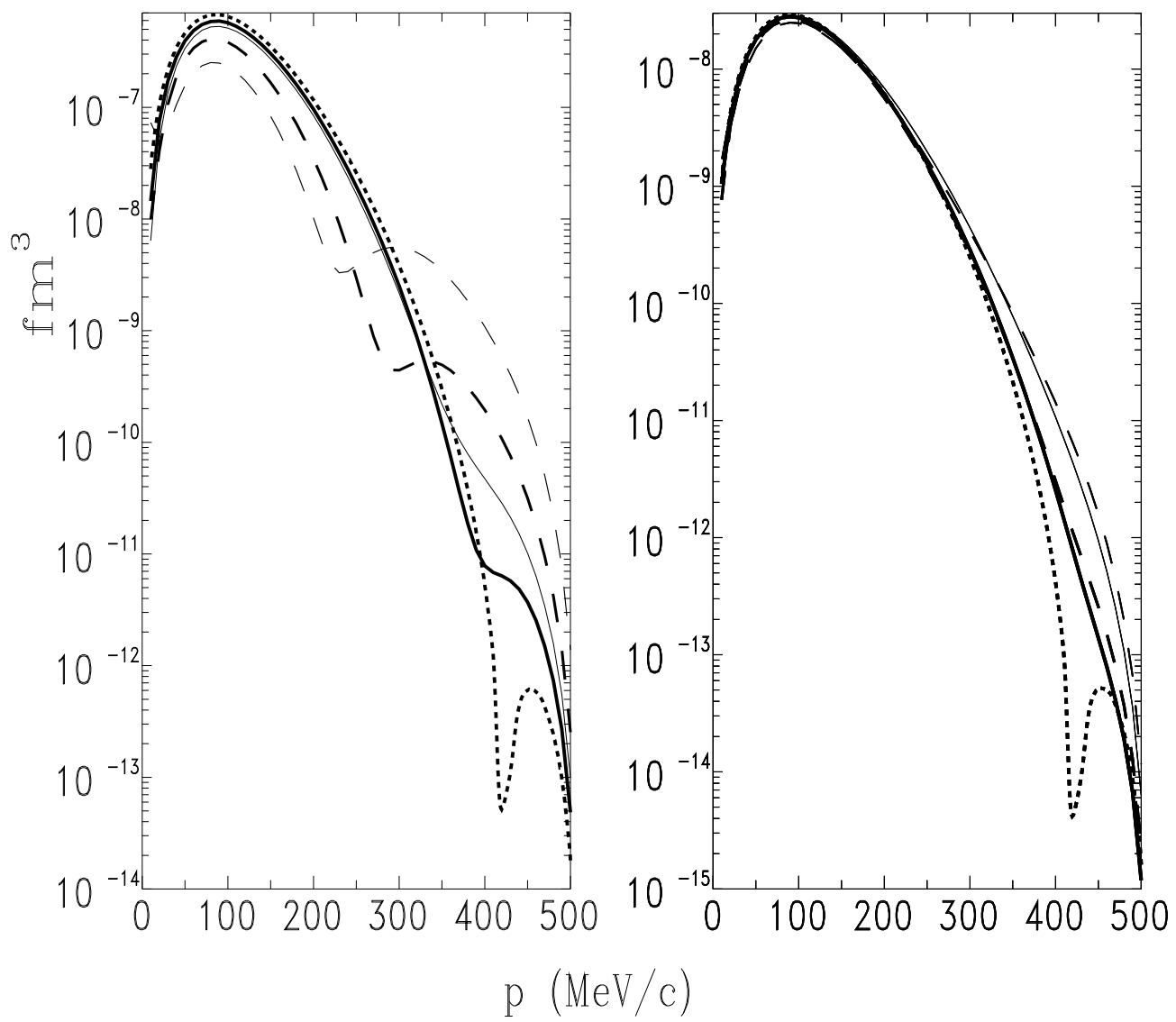


Figure 12

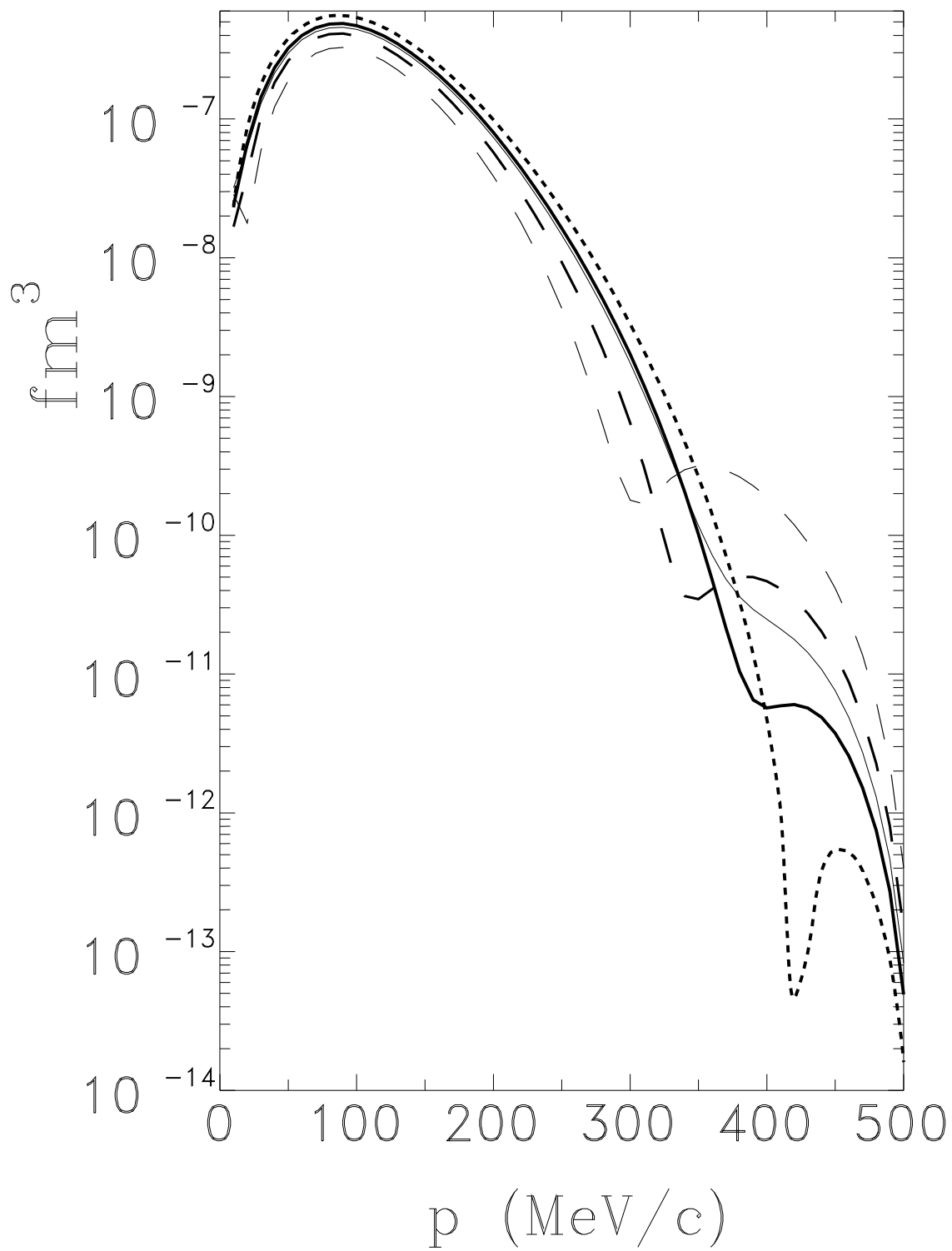


Figure 13

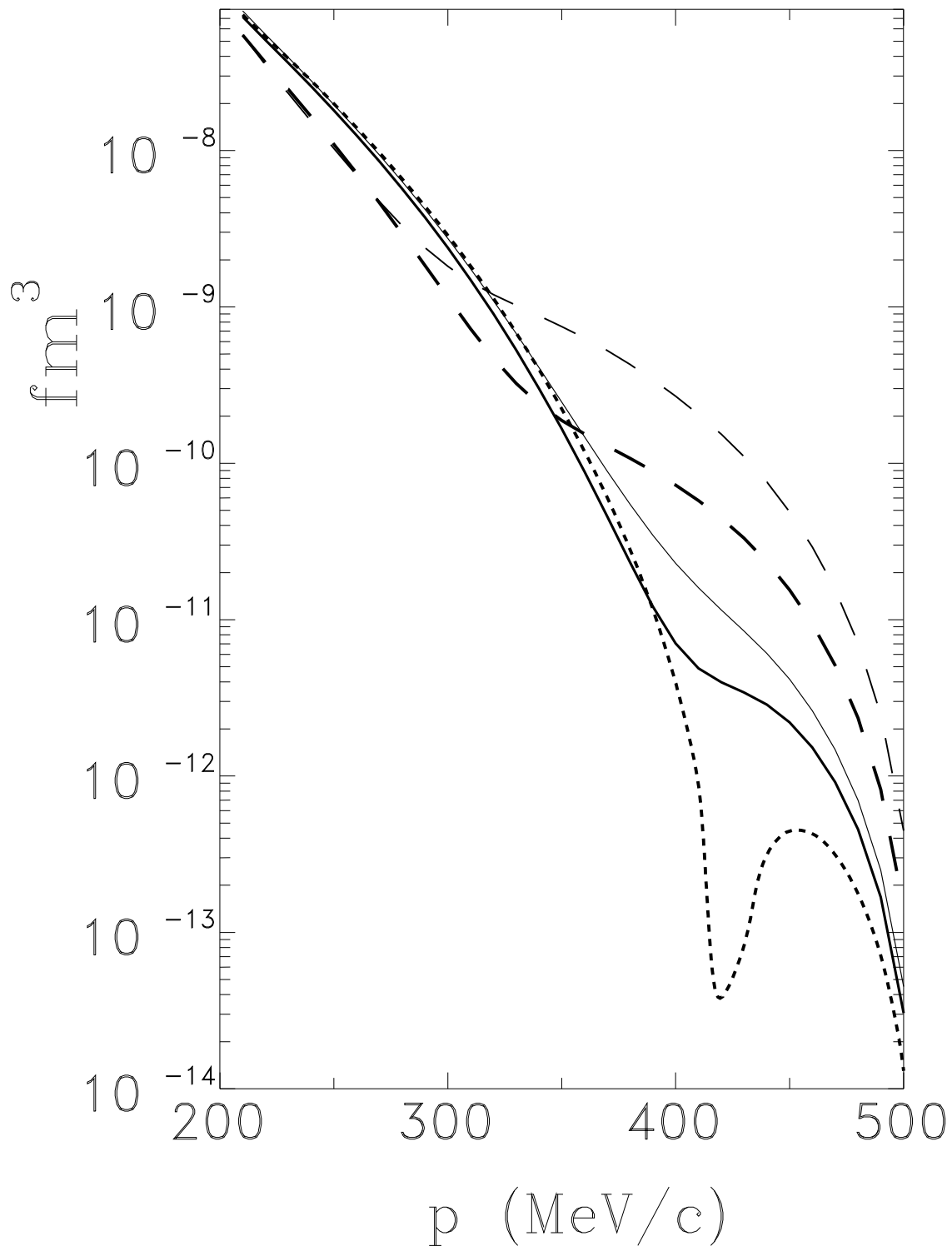


Figure 14